

**AN INVESTIGATION OF THE DELIQUESCENCE OF  
FERRICOPIAPITE AND THE ONSET OF  
DELIQUESCENCE OF EPSOMITE CRYSTAL FACES OF  
DIFFERING MILLER INDICES**

by

LOGAN ASTIN JAMESON

A thesis submitted to the Department of Geological Sciences and Geological  
Engineering in conformity with the requirements for the degree of Masters of  
Science

Queen's University

Kingston, Ontario, Canada

January, 2011

Copyright © Logan Astin Jameson, 2011

## ABSTRACT

Deliquescence is the process whereby a solid interacts with a humid atmosphere and begins to dissolve when the partial pressure of H<sub>2</sub>O in the atmosphere exceeds the partial pressure of H<sub>2</sub>O at which the solid is in equilibrium at a given temperature. Deliquescence of sulfate minerals poses a risk to both plant and animal life as metals and acid that are stored in the mineral structure are released. Detailed solid-solution transition boundaries for sulfate minerals aid in the understanding of acid mine waste behavior in the event of environmental changes. The deliquescence behaviors of ferricopiapite, melanterite, halite and epsomite have been studied as a function of temperature and relative humidity. A device has been developed to determine the onset of deliquescence as the temperature and/or relative humidity around a sample of sulfate mineral is varied. Experiments were conducted on several synthetic analogues of minerals. Ferricopiapite was studied as it is the most likely mineral to exhibit this behavior in common acid mine drainage sites where sulfates are present. Because no experimental data exist for the deliquescence of ferricopiapite, in order to properly test the device experiments in which the relative humidity was raised above the deliquescence point and then reversed were conducted using synthetic melanterite and halite for which solid-vapor equilibrium constants for temperature and relative humidity are known. Results of the reversal experiments for melanterite and halite show that the surface resistivity probe designed for this study accurately determines the onset of deliquescence as predicted by the known solid-liquid-vapor phase diagrams. The deliquescence of copiapite is not a reversible process as it does not re-precipitate from the liquid created by deliquescence as the relative humidity is lowered. Epsomite was studied to determine if there was any crystallographic control of the onset of deliquescence between different crystal faces. A significant and consistent difference in the onset of deliquescence was observed between the {111} and {100} faces with the {111} face always being the first to deliquesce as a function of increased relative humidity.

## **ACKNOWLEDGEMENTS**

I would like to thank Dr. Ron Peterson, my supervisor, for his knowledge, generous patience and the use of laboratory facilities.

I would like to thank Al Grant for his support with the use of the X-ray diffractometer, SEM and sharing his knowledge.

As well, I would like to thank Evelyne Leduc for her insight, help with lab equipment and support.

I would like to also thank Sarah Rice for all of her help and advice.

I would also like to thank Patrick van Kooten for all his advice, calm during stressful times and for always being there for me.

Thank you to my parents, for always encouraging and supporting me.

# TABLE OF CONTENTS

<b>ABSTRACT</b> .....	<b>I</b>
<b>ACKNOWLEDGEMENTS</b> .....	<b>II</b>
<b>LIST OF TABLES</b> .....	<b>IV</b>
<b>LIST OF APPENDICES</b> .....	<b>VII</b>
<b>DEFINITIONS</b> .....	<b>VIII</b>
<b>CHAPTER 1: INTRODUCTION</b> .....	<b>1</b>
<b>CHAPTER 2: MINERALOGY OF STUDY MINERALS</b> .....	<b>5</b>
FERRICOPIAPITE .....	5
MELANTERITE .....	5
HALITE .....	8
EPSOMITE .....	8
<b>CHAPTER 3: METHODS</b> .....	<b>13</b>
TEMPERATURE AND HUMIDITY CHAMBER DESIGN .....	14
SURFACE RESISTIVITY PROBE .....	19
TEMPERATURE AND HUMIDITY CHAMBER CONTROL .....	22
MINERAL SYNTHESIS .....	27
<b>CHAPTER 4: RESULTS</b> .....	<b>29</b>
FERRICOPIAPITE DELIQUESCENCE .....	29
<i>Melanterite Deliquescence</i> .....	36
<i>Halite Deliquescence</i> .....	40
EPSOMITE DELIQUESCENCE .....	46
<b>CHAPTER 5: DISCUSSION</b> .....	<b>52</b>
FERRICOPIAPITE DELIQUESCENCE .....	52
EPSOMITE DELIQUESCENCE .....	53
<b>CHAPTER 6: CONCLUSIONS</b> .....	<b>61</b>
FUTURE WORK .....	62
<b>REFERENCES</b> .....	<b>63</b>

## LIST OF TABLES

Table 1	Expected and measured relative humidity values for various salts at 30°C.	17
Table 2	Formulae used in the calculation of relative humidity.	18
Table 3	Results for the Sensirion (SHT 1X) relative humidity verification.	24
Table 4	Deliquescence points for ferricopiapite crust.	32
Table 5	Deliquescence points for melanterite.	39
Table 6	Deliquescence points for halite.	45
Table 7	Results of epsomite deliquescence experiments.	51

## LIST OF FIGURES

Figure 1	Stability phases of some Fe <sup>3+</sup> and Fe <sup>2+</sup> minerals.	3
Figure 2	Sample of ferricopiapite crust.	6
Figure 3	Atomic structure of ferricopiapite.	7
Figure 4	Hydrogen Bonding Scheme of epsomite.	10
Figure 5	Epsomite crystal illustrations.	11
Figure 6	Atomic structure of epsomite.	12
Figure 7	Temperature and Humidity Control Chamber.	15
Figure 8	Temperature and Humidity Control Chamber Component Placement.	20
Figure 9	View of surface resistivity probe.	21
Figure 10	Information flow in Temperature and Humidity Control Chamber.	26
Figure 11	Change in relative humidity over time for ferricopiapite experiment.	31
Figure 12	Ferricopiapite, melanterite and halite deliquescence points.	33
Figure 13	XRD scan of ferricopiapite crust after deliquescence and re-precipitation.	35
Figure 14	Change in relative humidity over time for melanterite experiment.	37
Figure 15	Stability field of melanterite.	38
Figure 16	Change in relative humidity over time for halite experiments at 30°C and 35°C.	41

Figure 17	Change in relative humidity over time for halite experiments at 40°C and 45°C.	42
Figure 18	Change in relative humidity over time for halite experiments at 50°C.	43
Figure 19	Deliquescence points for halite.	42
Figure 20	Synthesized epsomite crystal.	47
Figure 21	Stability field of epsomite.	48
Figure 22	Surface atoms for a particular slice, along the $m(110)$ face of epsomite as viewed 45° from the $a$ and $b$ axis	55
Figure 23	Surface atoms for cross section of the $m(110)$ face of epsomite as viewed down the $c$ axis.	56
Figure 24	Surface atoms for a particular slice, along the $l(111)$ face of epsomite as viewed perpendicular to the face.	57
Figure 25	Surface atoms for a particular slice, along the $l(111)$ face of epsomite as viewed perpendicular to the $c$ axis and 45° from the $a$ and $b$ axis.	58
Figure 26	Idealized diagram depicting dissolution pit formed on crystal surface upon initiation of deliquescence.	60

## LIST OF APPENDICES

- Appendix A Structural data for ferricopiapite crust from Rietveld refinement.
- Appendix B Structural data for melanterite from Rietveld refinement.
- Appendix C Technical data for Edgetech 2000™ Chilled Mirror Hygrometer.
- Appendix D Technical data for Basic Stamp 2™ module.
- Appendix E Technical data for Board of Education Development Board™.
- Appendix F Technical data for Sensirion SHT 1X™ temperature and humidity probe.

## DEFINITIONS

Deliquescence: The process by which a water soluble substance adsorbs moisture from the atmosphere and begins to dissolve in the adsorbed water and form a solution. Deliquescence occurs when the partial pressure of the H<sub>2</sub>O vapor in equilibrium with the saturated solution that is formed is less than the partial pressure of water vapor in the air (Encyclopedia Britannica, 2010)

## Chapter 1: Introduction

The study of minerals that form as a result of acid mine drainage (AMD) is important to the understanding of their impact on surrounding environments.

AMD is a result of the oxidation of sulfide-bearing minerals when they are exposed to oxygen and water. This exposure takes place both inside and on the surface of tailings piles and exposed mine workings. As a result of the oxidation of sulfide minerals and exposure to water which forms acid, AMD has a low pH and is characterized by high concentrations of heavy metals and other toxic elements which are harmful to plant and animal life (Akcil & Koldas, 2006).

When AMD minerals, which are water soluble, are exposed to humidity above their field of stability they deliquesce and form solutions containing acid,  $\text{SO}_4$ , Fe, Cd, As, Zn, Cu and  $\text{Fe}^{3+}$  (Jamieson et al., 2005). When these elements, metals and metalloids are external to an organism, they are unlikely to cause any adverse effect, but once absorbed may do so. In order for a metal or metalloid to come in contact with an organism or be made bioavailable for absorption by an organism, it must be transported to it. Such was the case with arsenic in drinking water in Bangladesh in the early 1970's, which caused poisoning and death (Adriano, 2001). To combat mobility of toxic elements, a greater understanding of the stability of AMD minerals is required.

Many studies have been performed that have examined the stability of acid mine drainage minerals at varying temperature and humidity (Posnjak & Merwin, 1922; Zodrow, 1980; Chou & Seal, 2002; Chou & Seal 2003). The stability ranges of various AMD minerals such as melanterite and epsomite group minerals have been determined (Chou and Seal, 2002; Chou and Seal 2003); however, there has been no work done to determine the stability of ferricopiapite  $[(\text{Fe})_{0.66}\text{Fe}_4(\text{SO}_4)_6(\text{OH})_2 \cdot 20 \text{H}_2\text{O}]$  as a function of temperature and relative humidity. Previous studies have focused on the stability of ferricopiapite in solution as a function of  $\text{H}_2\text{O}$ ,  $\text{Fe}_2\text{SO}_3$  and temperature (Posnjak & Merwin, 1922).

The stability fields of several  $\text{Fe}^{3+}$  minerals as a function of pH and  $p\epsilon$  have been calculated by Majzlan et al. (2006) and are shown in Figure 1. These stability fields are approximate as the speciation in such aqueous solutions could not be taken into account. There are two sulfur bearing species,  $(\text{SO}_4)^{2-}$  and  $(\text{HSO}_4)^-$ , which occur in concentrated aqueous solutions of pH ~ 1 at  $T = 298.15$  K at equal concentrations (Dickson et al., 1990). The calculations used to create the stability diagram only used one of the species,  $(\text{SO}_4)^{2-}$ . If  $(\text{HSO}_4)^-$  were used instead in the model, different boundaries would be produced (Majzlan et al., 2006). The experiments performed in our study seek to add to the information available on the phase boundaries of ferricopiapite through physical measurements.

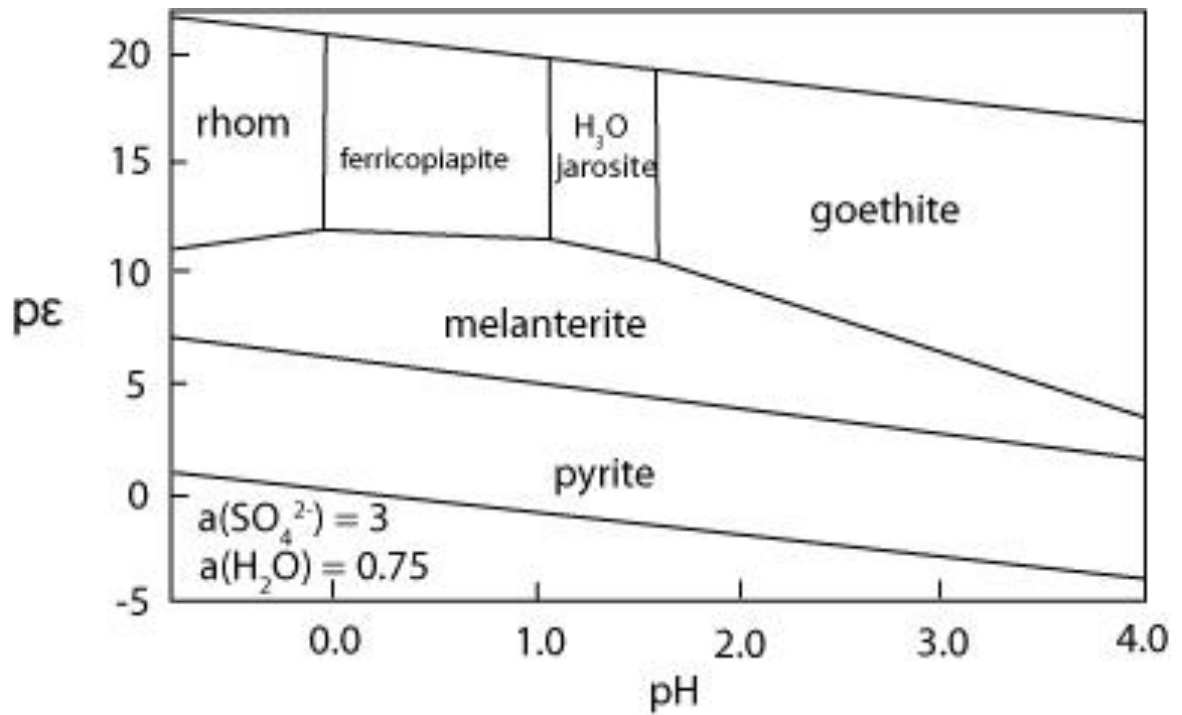


Figure 1 – Stability fields of some Fe<sup>3+</sup> and Fe<sup>2+</sup> sulfates. Abbreviations of phases: rhom = rhomboclase, H<sub>3</sub>O jarosite = hydronium jarosite (after Majzlan et al., 2006).

The copiapite group minerals are of the general formula  $XR_4(SO_4)_6(OH)_2 \cdot nH_2O$ . The X position can contain Fe, Al, Mn, Zn, Na, K, Co, Ca, Cu and others. R is dominantly  $Fe^{3+}$  and the upper limit of n is 20 (Zodrow, 1980). Copiapite group minerals are commonly found in mine tailings piles or as crust or aggregations on the surface of sulfide minerals. Protection from rainfall and transient surface flows increases the likelihood of copiapite group mineral growth (Jamieson et al., 2005).

No work has been done to determine if there is a difference in the onset of deliquescence between faces of different Miller indices on a single epsomite crystal. By studying epsomite, it was determined by Calleri (1984) that there are  $SO_4^{2-}$  groups on the  $\{-1,-1,-1\}$  face and  $(MgH_2O)_6^{2+}$  groups on the  $\{111\}$  face. It may also be possible that an increased abundance of hydrogen atoms available at one crystal face over another causes deliquescence to occur earlier, by allowing for a greater number of hydrogen bonds to form with oxygen in water vapor.

This study will use surface resistivity probes to determine the onset of deliquescence of ferricopiapite at various temperatures with studies of melanterite and halite to confirm the selected method of measurement. A second objective is to evaluate the effect of differing crystal faces on the onset of deliquescence.

## Chapter 2: Mineralogy of Study Minerals

### Ferricopiapite

Ferricopiapite is a member of the copiapite group of minerals and is commonly found associated with pyrite. It is a triclinic mineral with the formula  $(\text{Fe})_{0.66}\text{Fe}_4(\text{SO}_4)_6(\text{OH})_2 \cdot 20 \text{H}_2\text{O}$ . Ferricopiapite is yellow to yellow-orange in color and forms scaly or granular powdery aggregates (Gaines et al., 1997). A sample of synthesized ferricopiapite is shown in Figure 2. The atomic structure of ferricopiapite is shown in Figure 3. There are infinite chains of composition  $[\text{Fe}_4(\text{SO}_4)_6(\text{H}_2\text{O})_8(\text{OH})_2](\text{H}_2\text{O})_2$  and slabs of composition  $([\text{A}(\text{H}_2\text{O})_6](\text{H}_2\text{O})_4)$ . The cation that occupies the A site in the structure is coordinated octahedrally by  $\text{H}_2\text{O}$  molecules and form  $[\text{A}(\text{H}_2\text{O})_6]$  units. These units are connected to the other atoms within the structure by hydrogen bonds only (Majzlan & Michallik, 2007).

### Melanterite

Melanterite ( $\text{FeSO}_4 \cdot 7\text{H}_2\text{O}$ ) occurs as blue-green encrustations and stalactites, and well-formed crystals are rare (Frau, 2000). Melanterite is monoclinic, colorless to white or green, has a hardness of 2 and streaks white (Gaines et al., 1997). The  $\text{Fe}(\text{H}_2\text{O})_6^{2+}$  octahedra, the  $\text{SO}_4^{2-}$  tetrahedra and the



Figure 2 - Sample of ferricopiapite crust. The space between the ends of the probes on the surface of the crust is approximately 1mm. The crust is held in place by Plasticine™.

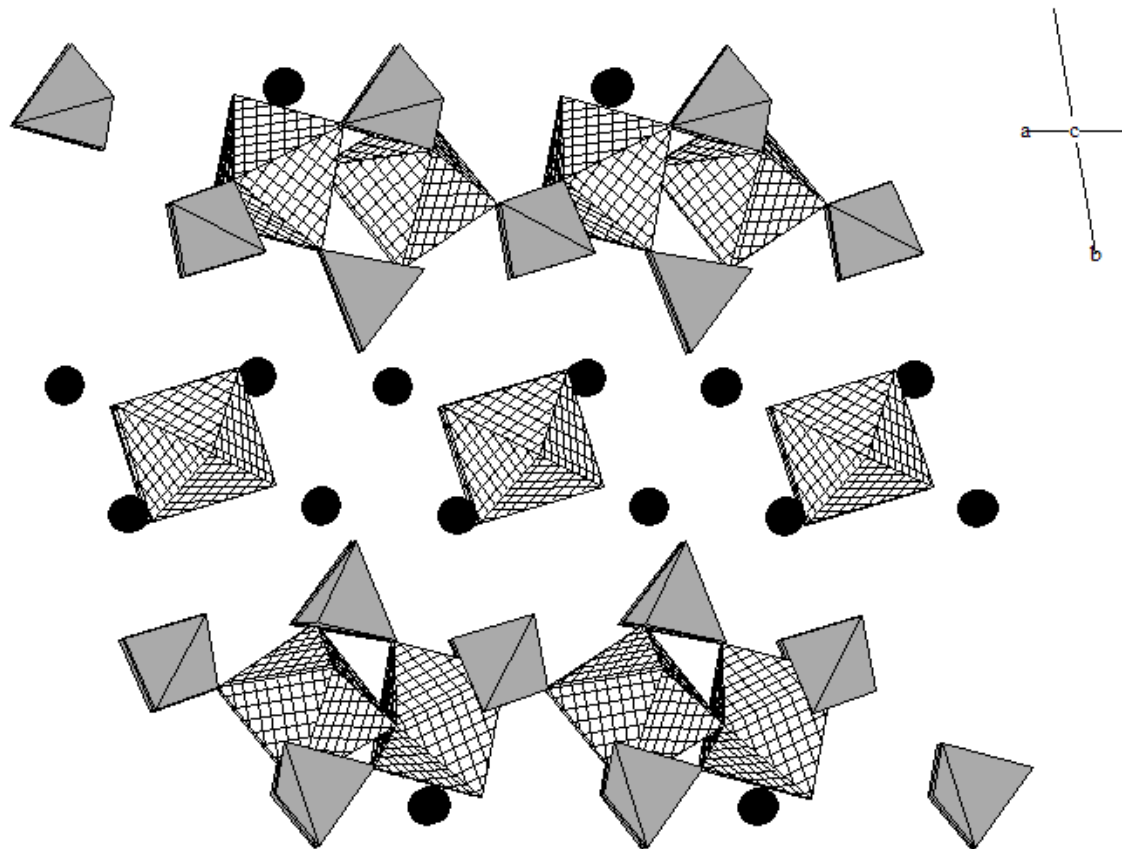


Figure 3 - Atomic structure of ferricopiapite (Majzlan et al., 2006). Hatched octahedra contain iron, grey tetrahedra contain sulfur, and black atoms are oxygen of H<sub>2</sub>O molecules; hydrogen atoms are not shown.

seventh water molecule, which is not coordinated to  $\text{Fe}^{2+}$ , are all connected together by hydrogen bonds (Baur, 1964).

## Halite

Halite ( $\text{NaCl}$ ) is a cubic mineral that exhibits cubic crystal form and rarely octahedral crystal form. It is normally transparent to translucent, colorless or may be yellowish, blue and purple or red. It has a hardness of 2.5 and streaks white. It occurs in evaporate deposits in saline lakes, bedded sedimentary deposits or as salt domes. Halite is water soluble (Gaines et al., 1997).

## Epsomite

Epsomite ( $\text{MgSO}_4 \cdot 7\text{H}_2\text{O}$ ) has a hardness of 2 – 2.5 and is white in color and streak. It is an orthorhombic mineral which has point group symmetry 2 2 2. Epsomite commonly forms as a crust or delicate fibrous efflorescence on walls of mine workings in coal or metal deposits (Gaines et al., 1997). The crystal forms exhibited by epsomite can be seen in Figure 4. The structure of epsomite has been shown to be composed of isolated  $\text{Mg}(\text{SO}_4)_2 \cdot 7\text{H}_2\text{O}$  ring molecules. These ring molecules are linked to each other by a three-dimensional network of hydrogen bonds (Baur, 1964). The hydrogen bonding network is shown in Figure

5. Six of the seven water molecules in the epsomite structure are coordinated to Mg; the seventh water molecule is not coordinated to either the magnesium or sulfur (Baur, 1964). The atomic structure of epsomite is shown in Figure 6.

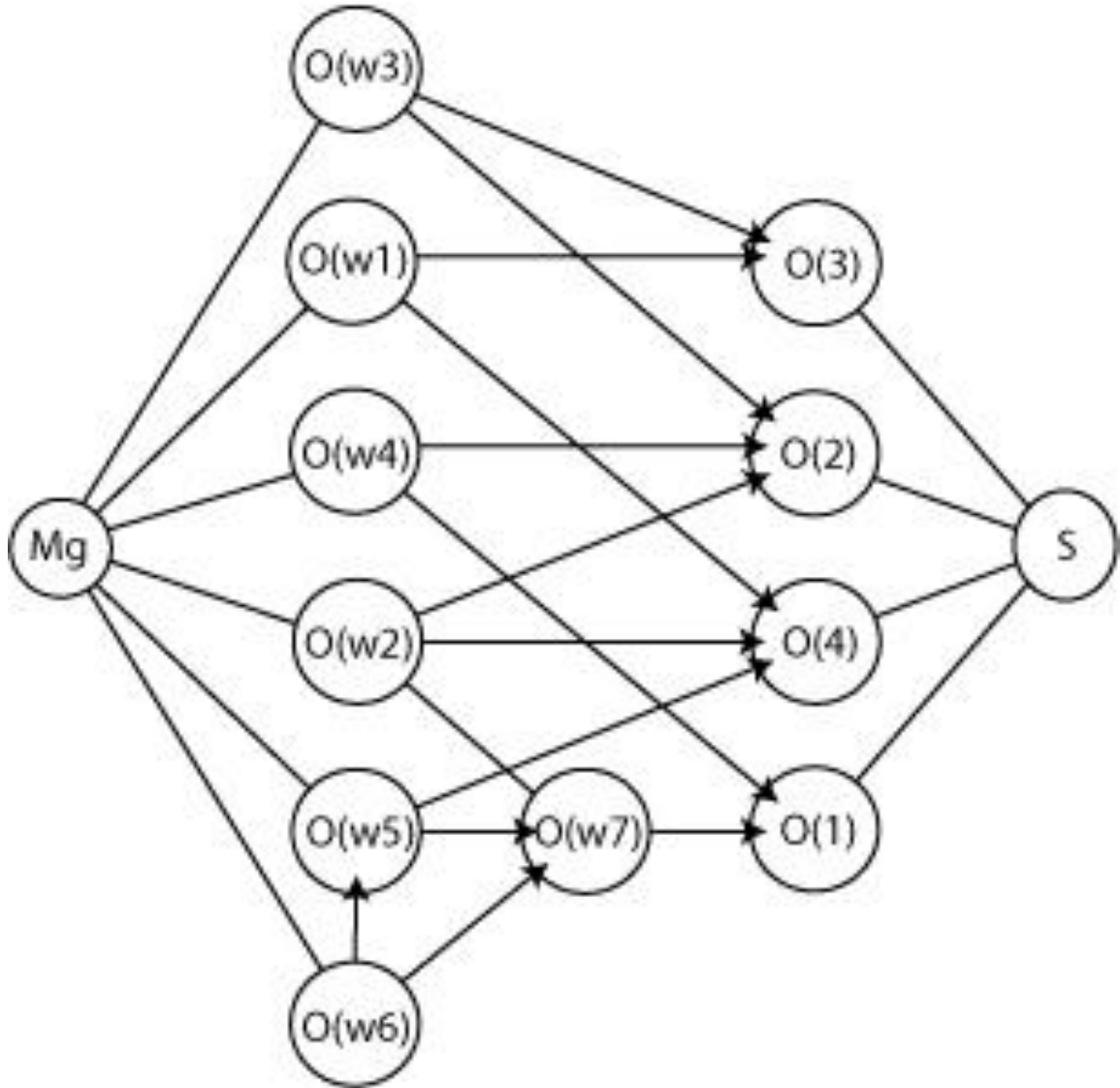


Figure 4 - Hydrogen bonding scheme of epsomite. O(w1) through O(w7) are water molecules, O(1) through O(4) are oxygen atoms that coordinate sulfur and participate in hydrogen bonds with water molecules in the structure (after Baur, 1964)

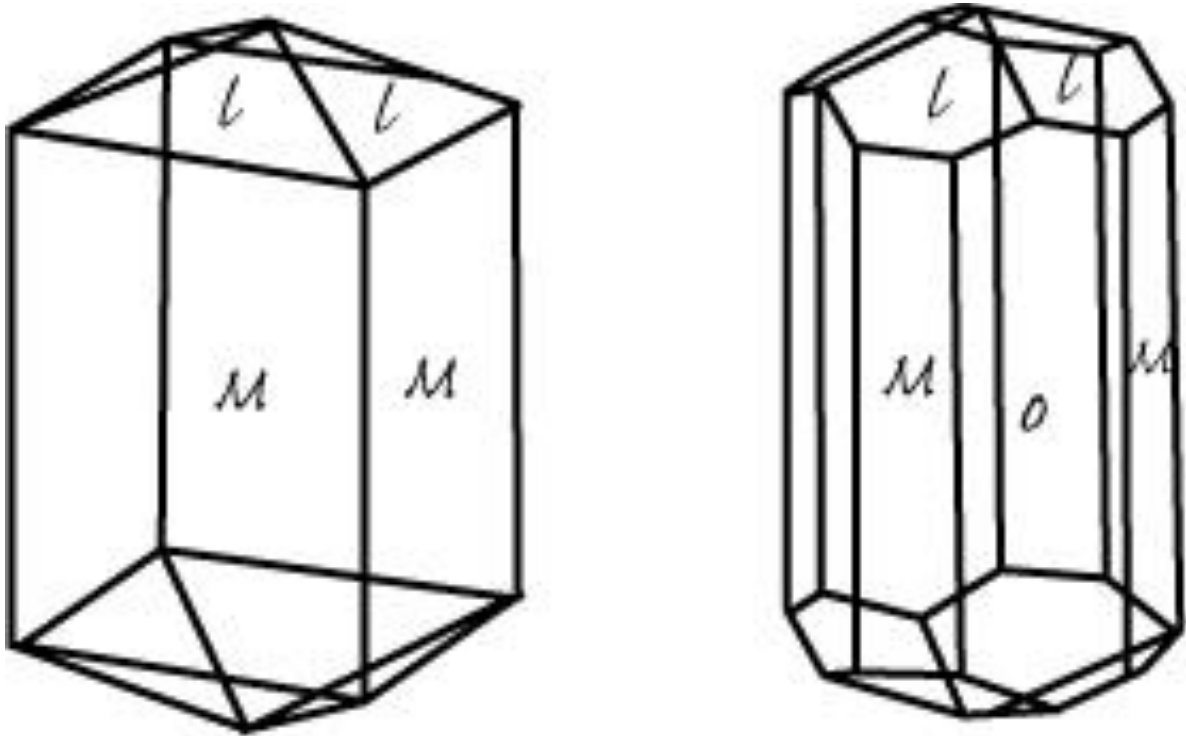


Figure 5 – Epsomite crystal forms. Depicted are;  $m\{110\}$ ,  $o\{010\}$ ,  $k\{111\}$  (after Haüy, 1823)

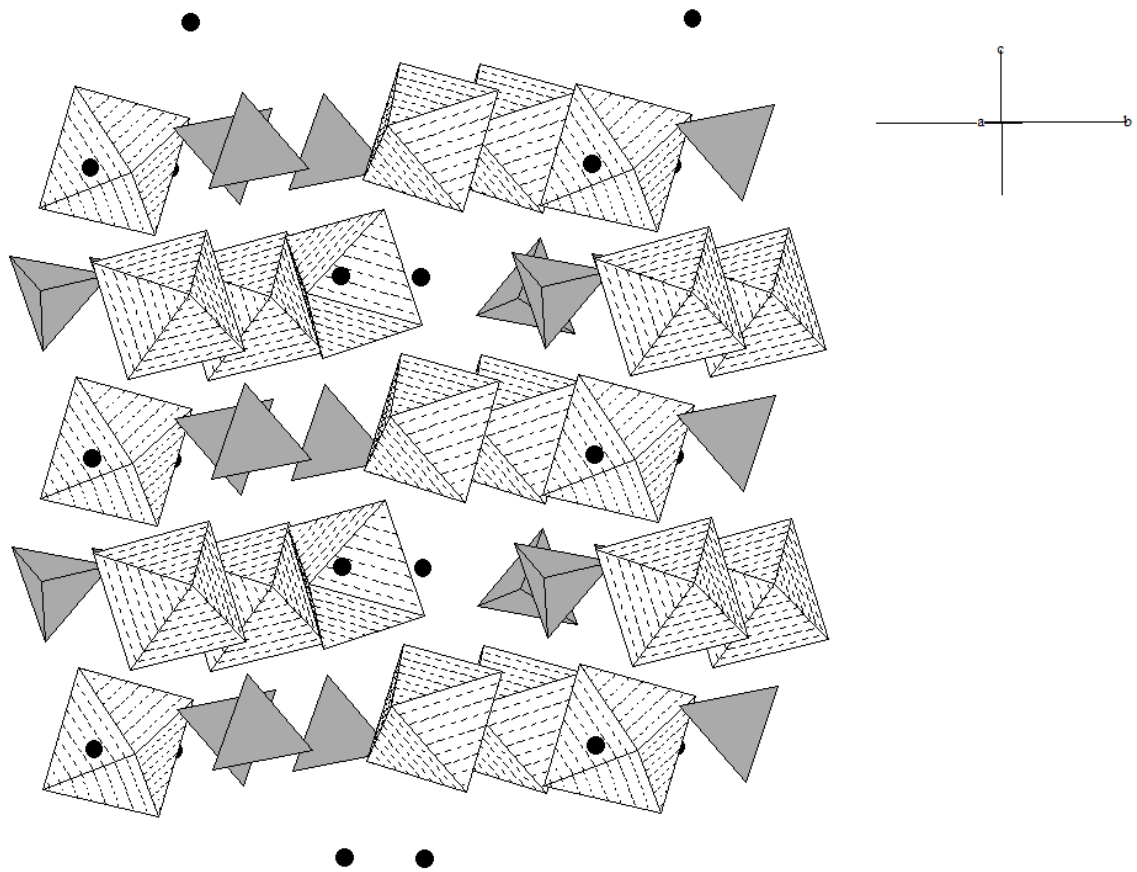


Figure 6 - Atomic structure of epsomite (Calleri et al., 1984). Black atoms are oxygen atoms of the water molecule that is not bonded directly to magnesium, dashed octahedra contain magnesium and grey tetrahedra contain sulfur. Hydrogen atoms are not shown.

## Chapter 3: Methods

In order to study the deliquescence of ferricopiapite, melanterite, halite and epsomite, a temperature and humidity controlled chamber was designed. The chamber was able to maintain a set temperature within, and had a system by which the relative humidity around a sample could be increased or decreased as was required. A second system was required that allowed for the study of the onset of deliquescence on the surface of a sample. As a mineral sample deliquesces, a solution forms on the surface which lowers resistance to the passage of electrical current. To measure this resistance, a surface resistivity probe was designed. Deliquescence is known to have occurred when a measurable resistance is detected.

Ferricopiapite was studied to determine the solid/solution boundary for a range of temperatures from 30°C to 50°C. Samples of ferricopiapite crust were inserted into the surface resistivity probe chamber and placed in contact with the wires of the probe. Relative humidity within the chamber was increased while the resistance between the two wires of the probe was monitored.

Two experiments were done to demonstrate the accuracy of the surface resistivity probe in determining onset of deliquescence of a mineral. Melanterite and halite were used in the experiments as they had been previously studied in Chou & Seal (2002) and Greenspan (1976) respectively. Both studies produced

graphs of temperature/Rh and solid/solution boundaries for their respective minerals. Using a mineral for which the temperature/Rh, solid/solution boundary is already known confirmed the precision and accuracy of the experimental setup. The halite experiment determined the deliquescence point of the mineral for both increasing and decreasing relative humidity at constant temperature and showed that the deliquescence points obtained while increasing the relative humidity were the same as those obtained when decreasing the relative humidity, within error.

## Temperature and Humidity Chamber Design

The chamber, shown in figure 7, was constructed of extruded polystyrene and sealed at the joints with silicone. The entire assembly was enclosed in 4 cm thick dense Styrofoam™. The two openings on the front of the box are for hand access to the chamber inside. Temperature inside the chamber was regulated by a 40W light bulb in response to sensor control. Two 12V fans were placed in the chamber to provide air circulation to ensure even temperature distribution. Relative humidity was controlled through the use of a salt buffer solution and a silica gel desiccant, which were both housed in PVC containers. The containers were connected by way of plastic tubes through which air passes to another PVC container that holds the sample to be tested. The sample container could be bypassed to allow sample exchange using valves in the air lines depending on the experiment being performed.

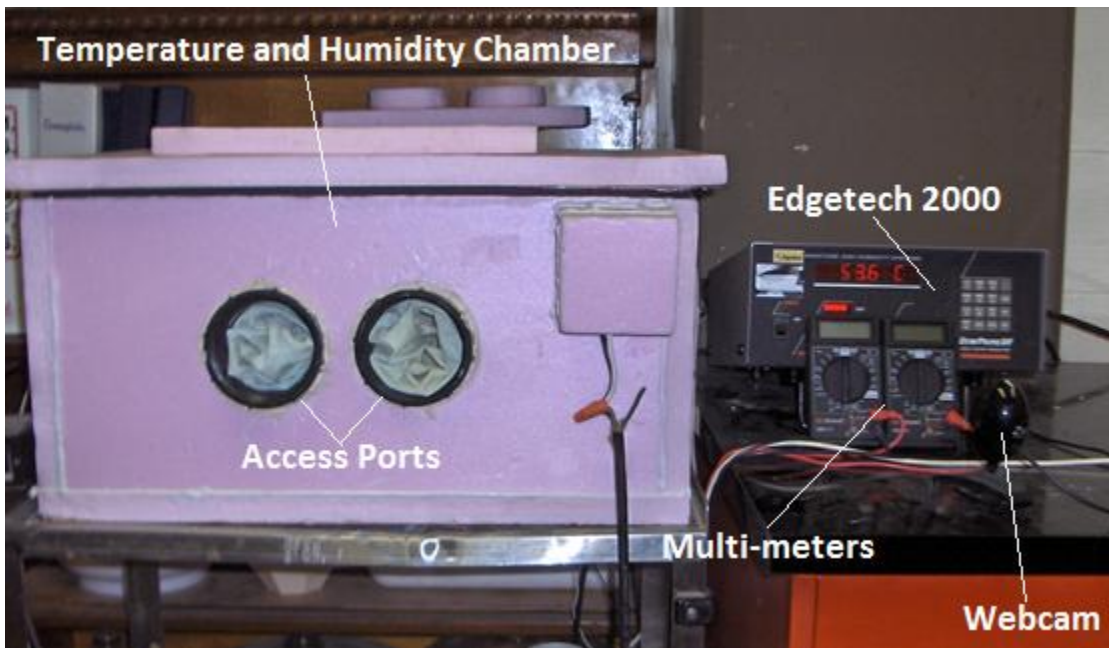


Figure 7 - Temperature and humidity control chamber. Edgetech 2000 hygrometer and two multi-meters to the right.

The sample container gas passes through the air lines to the sensor of an Edgetech 2000 chilled mirror hygrometer. The dew point temperature accuracy of the Edgetech 2000 is +/- 0.2 °C (Appendix C). The chilled mirror hygrometer determines dew point temperature by measuring the degradation of a laser reflection off a mirror, caused by condensation on the mirror surface. The temperature of the mirror is cycled to evaporate and condense the vapor in the atmosphere onto the mirror surface. This accuracy was verified using MgCl<sub>2</sub>, NaCl and K<sub>2</sub>SO<sub>4</sub> (Table 1) inserted into the buffer solution position in the chamber, prior to initiation of experiments. The relative humidities produced by these buffers are well known (Greenspan, 1976). The displays of the Edgetech 2000 hygrometer and multi-meters were captured on a continuously recording camera. Images showed both digital multi-meters, the dew point of the sample chamber as measured by the Edgetech 2000 hygrometer, and the date and time. The dew point temperature reading from the hygrometer is used to calculate relative humidity (calculation listed in Table 2).

<b>Buffer Salt</b>	<b>Temperature</b>	<b>Greenspan %RH</b>	<b>Observed %RH</b>
MgCl <sub>2</sub>	30°C +/- 0.4°C	32.4 +/- 0.14	32.3 +/- 1.1
NaCl	30°C +/- 0.4°C	75.1 +/- 0.11	75.1 +/- 1.1
K <sub>2</sub> SO <sub>4</sub>	30°C +/- 0.4°C	97.0 +/- 0.40	96.6 +/- 1.1

Table 1 - Expected and measured relative humidity values for various salts at 30°C. Expected %RH values are from Greenspan (1976). Error for Observed %RH was determined by propagating the error for the Edgetech 2000 chilled mirror hygrometer and the Sensirion SHT 1x.

$f = E_s / E * 100$	f = relative humidity
$E_s = 6.11(10^{7.5T_{dc} / 237.7 + T_{dc}})$	$E_s$ = actual vapor pressure Tdc = dew point temperature in degrees Celsius
	6.11 is the pressure coefficient for standard atmosphere
$E = 6.11(10^{7.5T_c / 237.7 + T_c})$	E = saturation vapor pressure Tc = air temperature in degrees Celsius

Table 2 - Formulae used in the calculation of relative humidity (National Physical Laboratory, 2010).

Gas flows from the Edgetech 2000 sensor to the humidity buffer chamber, where it equilibrates with the solution and is passed to the sample container and back to the Edgetech to complete the gas circuit. Figure 8 shows the placement and connections within the temperature and humidity control chamber. The rate of increase or decrease of relative humidity in the system is controlled by increasing or decreasing the air flow through either the desiccant or the buffer solution.

## Surface Resistivity Probe

In order to study the deliquescence of crystal faces, compact powders or crusts, a special system was designed, part of which is shown in Figure 9. The system for the study of ferricopiapite, melanterite and halite uses two sets of two wires. The wires were 0.1 mm steel spring wire and were mounted in silicone, such that they pressed lightly against the surface of the minerals to ensure contact.

When the wires were placed on the surface of the crystal, compact powder or crust, the tips were a distance of ~1mm apart. The wires were replaced at 4 day intervals to ensure there was no rust which could cause signal degradation. The resistance between the two wires was measured by a digital

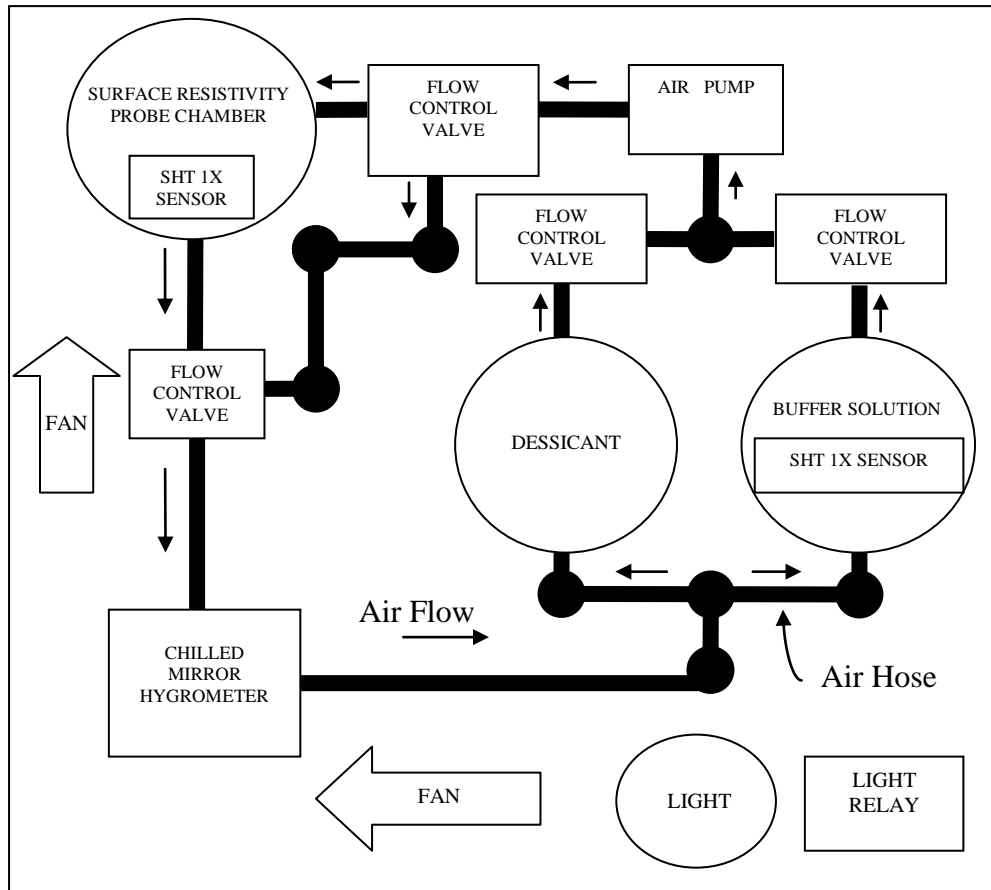


Figure 8 - Placement and connections of components within the temperature and humidity control chamber. The SHT1X sensors and the light relay are connected electronically to the microcontroller. The temperature for the system is monitored at the surface resistivity probe chamber. Image is not to scale.

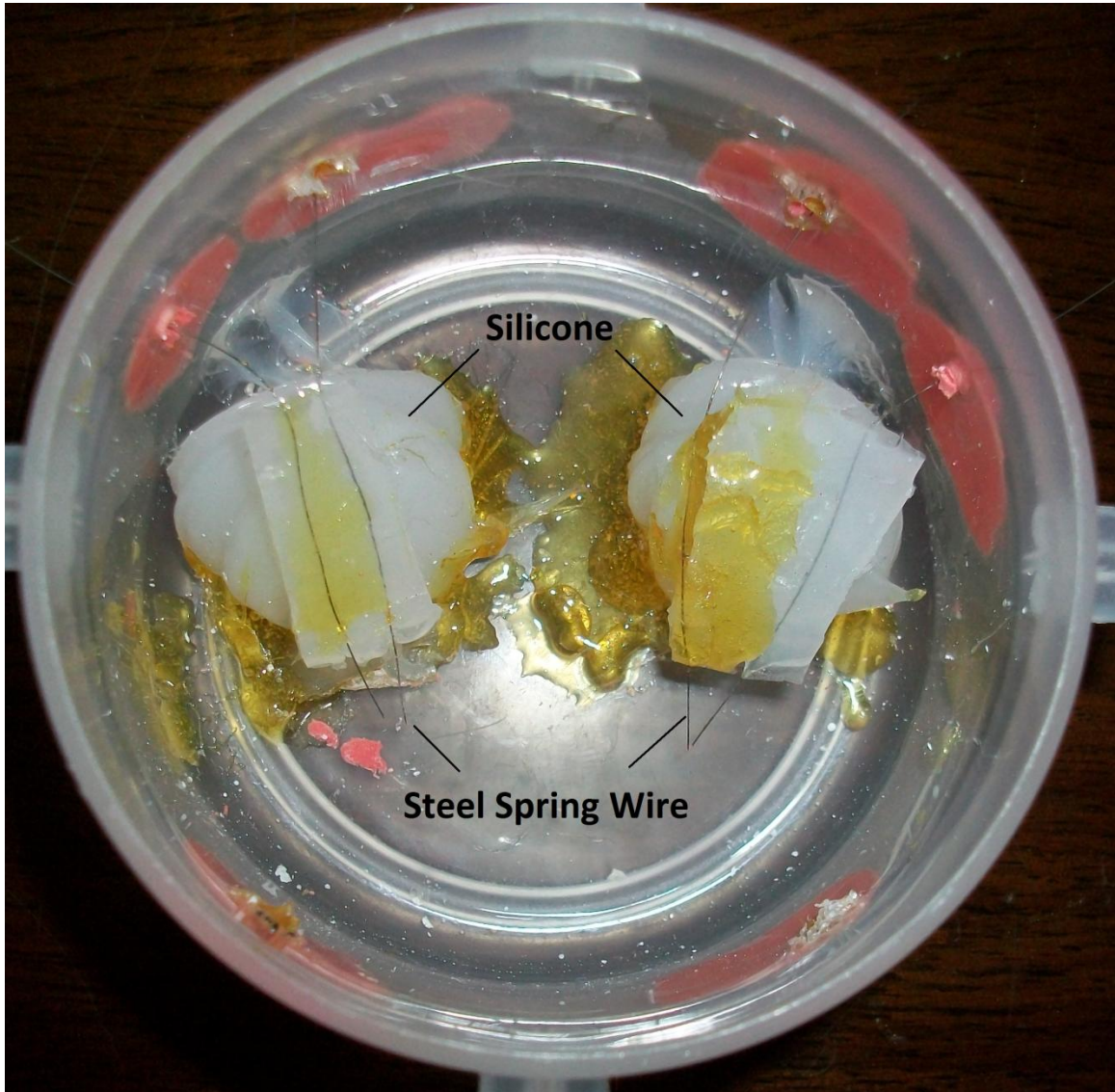


Figure 9 - View of the surface resistivity probes. No crystals are present. The diameter of the chamber is 7.5cm.

multi-meter. When the sample was inserted into the sample chamber and the wires placed on the surface, the digital multi-meter measured an infinite resistance because it was an open circuit and the substance was an insulator. When the sample began to deliquesce, a film of solution appeared on the surface of the mineral. This film of saturated brine contacted both wires and allowed for the circuit to close, resulting in a resistance reading on the digital multi-meter.

Only one digital multi-meter was used for the ferricopiapite, melanterite and halite experiments while two were used for the epsomite experiment, one for each crystal face being studied. The temperature and relative humidity experienced by each face was the same as they were close to each other and the humid air entered and left the chamber from points equidistant from both samples. The two sets of wires measured the response of two different crystal faces of different Miller indices which were not related by the symmetry of the material. Epsomite samples were mounted and mostly covered with Plasticine™ to limit the exposure area to 0.5 x 0.5 centimeters which ensured consistent exposure of the selected faces.

## Temperature and Humidity Chamber Control

To ensure stability in the experiments, the temperature and humidity within the system was precisely controlled. To control the temperature a BASIC Stamp Microcontroller™ (Parallax Incorporated) and a Board of Education Development

Board™ (Parallax Incorporated) were used. The information for both of these products is included in Appendix D and E respectively.

The Board of Education Development Board™ was connected to two temperature and humidity chips from Sensirion Incorporated (SHT 1X), these chips have a temperature accuracy of  $\pm 0.4^{\circ}\text{C}$  and a claimed relative humidity accuracy of  $\pm 3.0\%$ . The data sheet for this chip is included in Appendix F. These values were verified by placing a temperature probe that uses the same Sensirion chip into the chamber for a 24 hour period. The chamber was set to a temperature of  $25.0^{\circ}\text{C}$  and all of the Sensirion chips measured the temperature as exactly  $25.0^{\circ}\text{C}$ . The relative humidity precision of the Sensirion chips was tested by placing them above saturated salt solutions in a sealed container. The relative humidity in the air above saturated salt solutions as a function of temperature is well known for common salts (Greenspan, 1976). The results of this experiment are included in Table 3. Although the Sensirion chips are capable of measuring relative humidity, they were not used to do so as it was determined that the error was in some cases greater than  $\pm 3\%$  relative humidity.

One of the chips was placed in the humidity buffer container whereas the other was placed in the sample container; they served to verify uniform temperature throughout the chamber. The chips were monitored using a computer that also set the temperature in the chamber.

Probe	Buffer	Temp (°C) (controlled)	Measured Humidity (%RH)	Greenspan Humidity (%RH)	Offset (%RH)	Temp (°C) (controlled)	Measured Humidity (%RH)	Ideal Humidity (%RH)	Offset (%RH)
A	KCl	23.5	84.0	84.5	-0.5	23.5	84.0	84.50	-0.50
C	KCl	23.0	79.5	84.5	-5.0	23.5	78.0	84.50	-6.50
D	KCl	23.0	83.0	84.5	-1.5	23.5	81.5	84.50	-3.00
E	KCl	23.0	82.5	84.5	-2.0	23.5	82.0	84.50	-2.50
F	KCl	23.0	85.5	84.5	1.0	23.5	85.5	84.50	1.00
A	NaCl	23.0	74.5	75.5	-1.0	21.5	74.0	75.50	-1.50
C	NaCl	23.0	71.0	75.5	-4.5	23.0	70.5	75.50	-5.00
D	NaCl	23.0	73.0	75.5	-2.5	23.5	72.0	75.50	-3.50
E	NaCl	23.0	72.5	75.5	-3.0	23.0	72.5	75.50	-3.00
F	NaCl	23.5	75.5	75.5	0.0	23.0	76.0	75.50	0.50
A	KI	23.0	70.0	69.5	0.5	23.5	70.5	69.00	1.50
C	KI	23.0	67.0	69.5	-2.5	23.0	68.0	69.50	-1.50
D	KI	23.0	68.5	69.5	-1.0	23.0	69.0	69.50	-0.50
E	KI	23.0	68.5	69.5	-1.0	23.0	68.5	69.50	-1.00
F	KI	23.0	72.5	69.5	3.0	23.5	73.0	69.50	3.50
A	NaBr	24.0	59.0	58.0	1.0	24.0	58.0	58.00	0.00
C	NaBr	23.5	57.5	58.0	-0.5	24.5	56.5	58.00	-1.50
D	NaBr	23.5	60.5	58.0	2.5	23.0	60.5	58.00	2.50
E	NaBr	24.0	58.5	58.0	0.5	23.5	55.5	58.00	-2.50
F	NaBr	23.0	63.5	58.0	5.5	23.0	63.5	58.00	5.50

Table 3 - Results for the Sensirion (SHT 1X) relative humidity verification. Ideal humidity results are from Greenspan (1976).

A program was written in BASIC Stamp Editor Version 2.2.6, in the Pbasic™ language, which allowed for the setting and monitoring of temperature in the chamber. The program communicated with the microcontroller to read the information that came from the temperature/humidity chips and then converted the information received from the microcontroller into temperature values. The program also instructed the microcontroller when to activate the light relay, which turned on a 40 watt light bulb used to heat the chamber and was connected via relay to the microcontroller. The general flow of data from the microcontroller to the various parts can be seen in Figure 10.

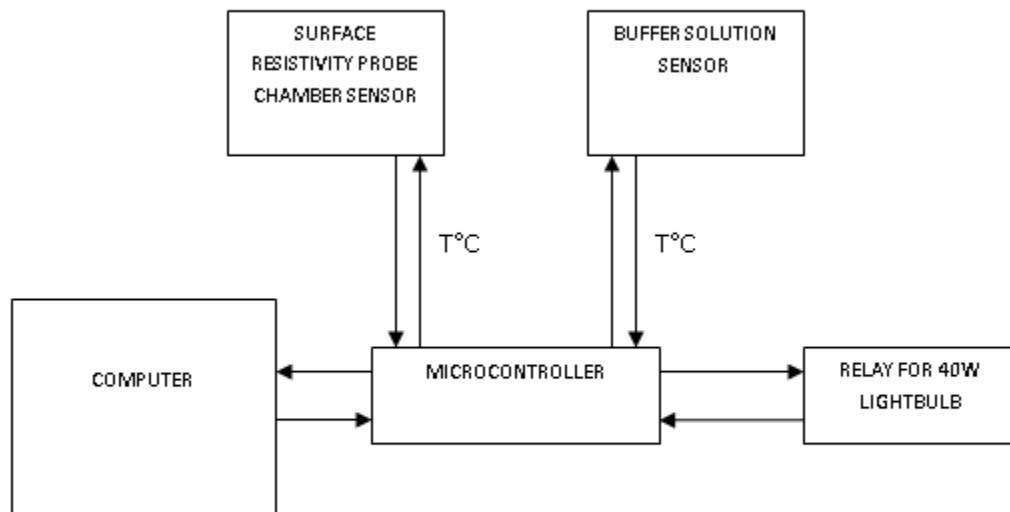


Figure 10 - Information flow in the temperature and humidity control chamber.

## Mineral Synthesis

Ferricopiapite was synthesized using reagent grade Alfa Aesar  $\text{Fe}_2\text{SO}_4 \cdot 5\text{H}_2\text{O}$  and distilled water. 40g of  $\text{Fe}_2\text{SO}_4 \cdot 5\text{H}_2\text{O}$  was added to 19 g of water inside a Fisher Scientific 125 ml Nalgene polypropylene wide mouth bottle and stirred until all the reagent was in solution (Friedlander et al., 2007). The solution, which had a pH of 1, was left standing open to air to allow ferricopiapite precipitation. Ferricopiapite formed a hard crust on the bottom of the bottle after all the water had evaporated from the solution. This synthesized ferricopiapite was analyzed using powder X-ray diffraction and the Rietveld method (Young, 1995) to confirm the identity of the product. Scan and structural data obtained from the Rietveld refinement are included as Appendix A.

Melanterite was synthesized using the method outlined by Anderson (2007). 30g of reagent grade  $\text{FeSO}_4 \cdot 7\text{H}_2\text{O}$  was added to 0.1M  $\text{H}_2\text{SO}_4$  to equal 60ml. The solution was heated while being stirred to ensure complete dissolution of the reagents. The heat did not exceed 70°C to prevent oxidation of the iron. After heating, the solution was left open to room air to allow for evaporation and precipitation of melanterite over seven days. Powder X-ray diffraction and Rietveld analysis was performed on the synthesized melanterite and the structural data is included as Appendix B.

Halite was synthesized by adding reagent grade NaCl to 40ml of distilled water at a temperature of 25°C in a beaker until saturated. The solution was stirred constantly while the reagent was added to ensure complete dissolution. The beaker was left open to atmosphere to allow for evaporation and precipitation. Powder X-Ray diffraction was done on the synthesized crystals to confirm that they were halite.

Epsomite was synthesized by adding reagent grade  $\text{MgSO}_4 \cdot 7\text{H}_2\text{O}$  to 300ml of distilled water in a beaker until the water was saturated. The solution was stirred constantly during addition of the reagent to ensure complete dissolution. The beaker was then left open to air so evaporation and precipitation would occur. Powder X-Ray diffraction was performed on the resulting crystals to confirm they were epsomite. Crystals of 1-2 cm dimensions were obtained and a sample can be seen in Figure 20.

## Chapter 4: Results

### Ferricopiapite Deliquescence

Small pieces of the ferricopiapite crust were removed from the bottle and the smooth side of the crust that was in contact with the bottle was used as the surface to sense deliquescence. Using the surface that formed by contact with the bottle ensured that the sample was relatively smooth and compact and there were no disruptions in the material between the wires measuring resistivity. The pieces of ferricopiapite crust were placed into the surface resistivity probe chamber. A buffer solution of KCl produced a humidity of 86% at 30°C and 82% at 50°C. The humid air from the buffer solution was mixed with dry air to achieve the desired relative humidity in the sample chamber.

When attempting to determine at what humidity a solid deliquesced, the rate of increase of the relative humidity in the chamber needed to be low enough that the system did not overshoot the relative humidity at which deliquescence occurs. A low rate of change was considered to be an increase of less than 3.5% RH over 6 hours. By keeping the rate of relative humidity increase low, the mineral surface experienced the same, or close to the same, relative humidity as measured by the sensor. Figure 11 shows the change in relative humidity over time for the ferricopiapite experiment. The deliquescence points obtained are

listed in Table 4 and shown compared against values obtained for melanterite and halite in Figure 12.

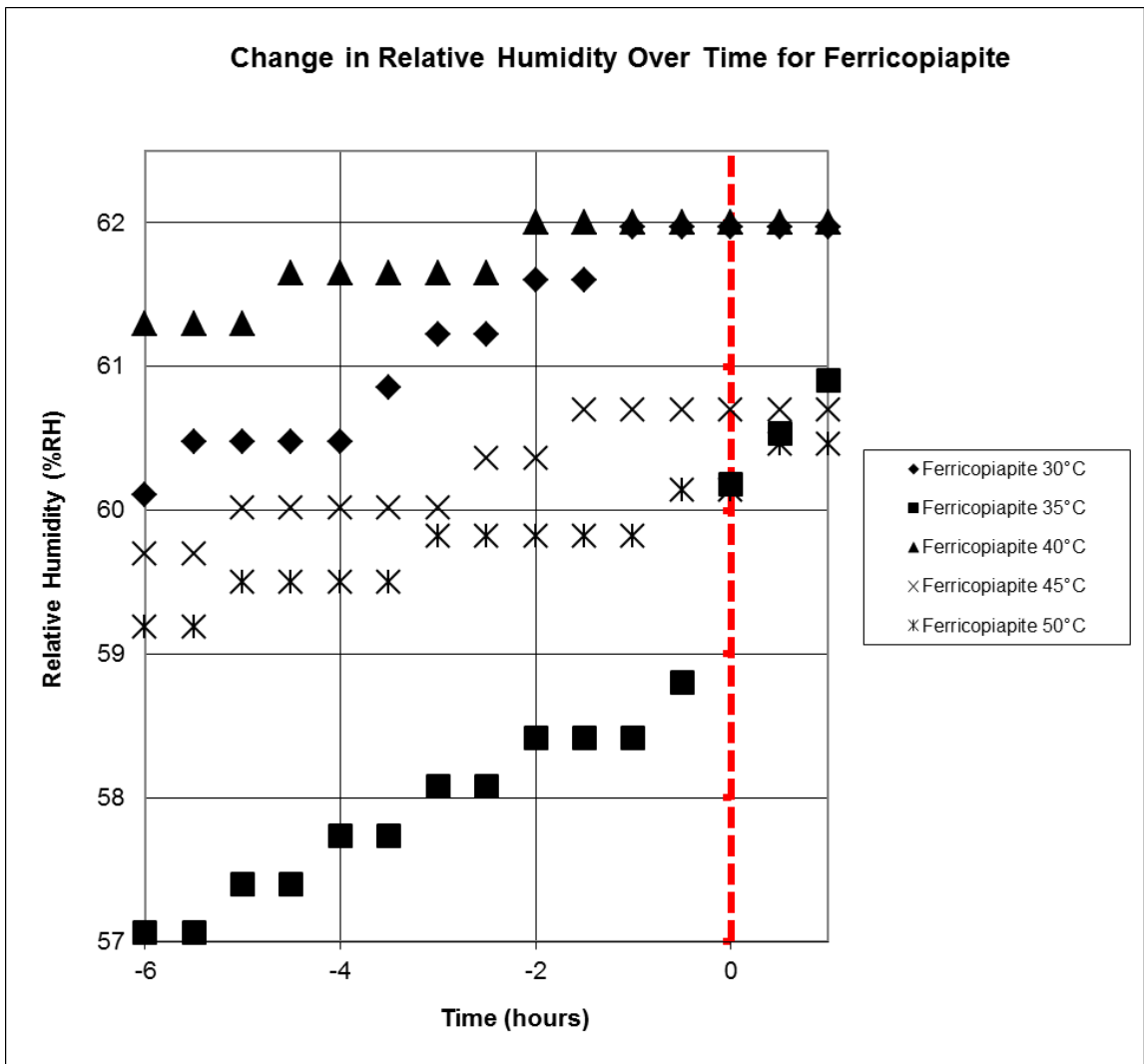


Figure 11 – Change in relative humidity over time for ferricopiapite experiment. Negative time values are time before deliquescence occurs. Deliquescence begins at zero hours and is indicated by the dashed vertical line.

Temperature (°C)	Deliquescence Humidity (%RH)
30	62.0 +/- 1.1
35	60.2 +/- 1.2
40	62.0 +/- 1.3
45	60.7 +/- 1.5
50	60.1 +/- 1.6

Table 4 - Deliquescence points for ferricopiapite crust at various temperatures. Measured at constant temperature and increasing relative humidity. Error was determined by propagating the error for the Edgetech 2000 chilled mirror hygrometer and the Sensirion SHT 1x through the formulae for calculation.

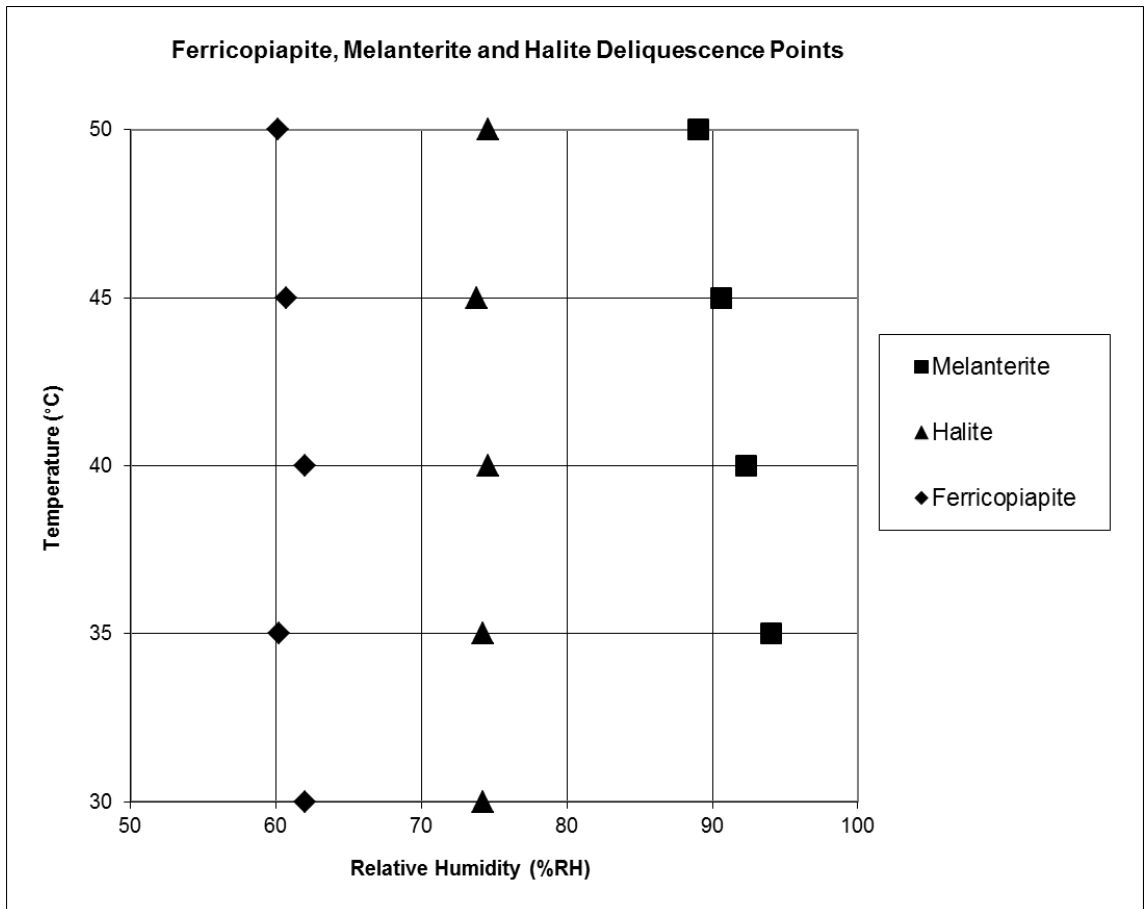


Figure 12 - Ferricopiapite, melanterite and halite deliquescence points obtained in this experiment.

In order to confirm that the deliquescence points from the experiment are correct, the method used to obtain them was verified. The method was verified using melanterite with increasing relative humidity; however for complete verification, deliquescence points must be obtained with decreasing relative humidity and show that identical values are obtained for a reversal of the process. In order to perform a reversal experiment, ferricopiapite must re-precipitate out of the solution formed during deliquescence. A sample of ferricopiapite was allowed to completely dissolve into solution before the relative humidity was lowered and the sample re-precipitated into a small amount of crystalline material. The XRD scan of the ferricopiapite crust after deliquescence and re-crystallization is included in Figure 13. The scan was analyzed using the International Center for Diffraction Data database, and no ferricopiapite or other mineral could be identified. Because ferricopiapite does not re-precipitate out of the solution formed by its deliquescence, it was not possible to determine the deliquescence point during decreasing relative humidity for ferricopiapite. To test the method used to determine deliquescence points, halite was used.

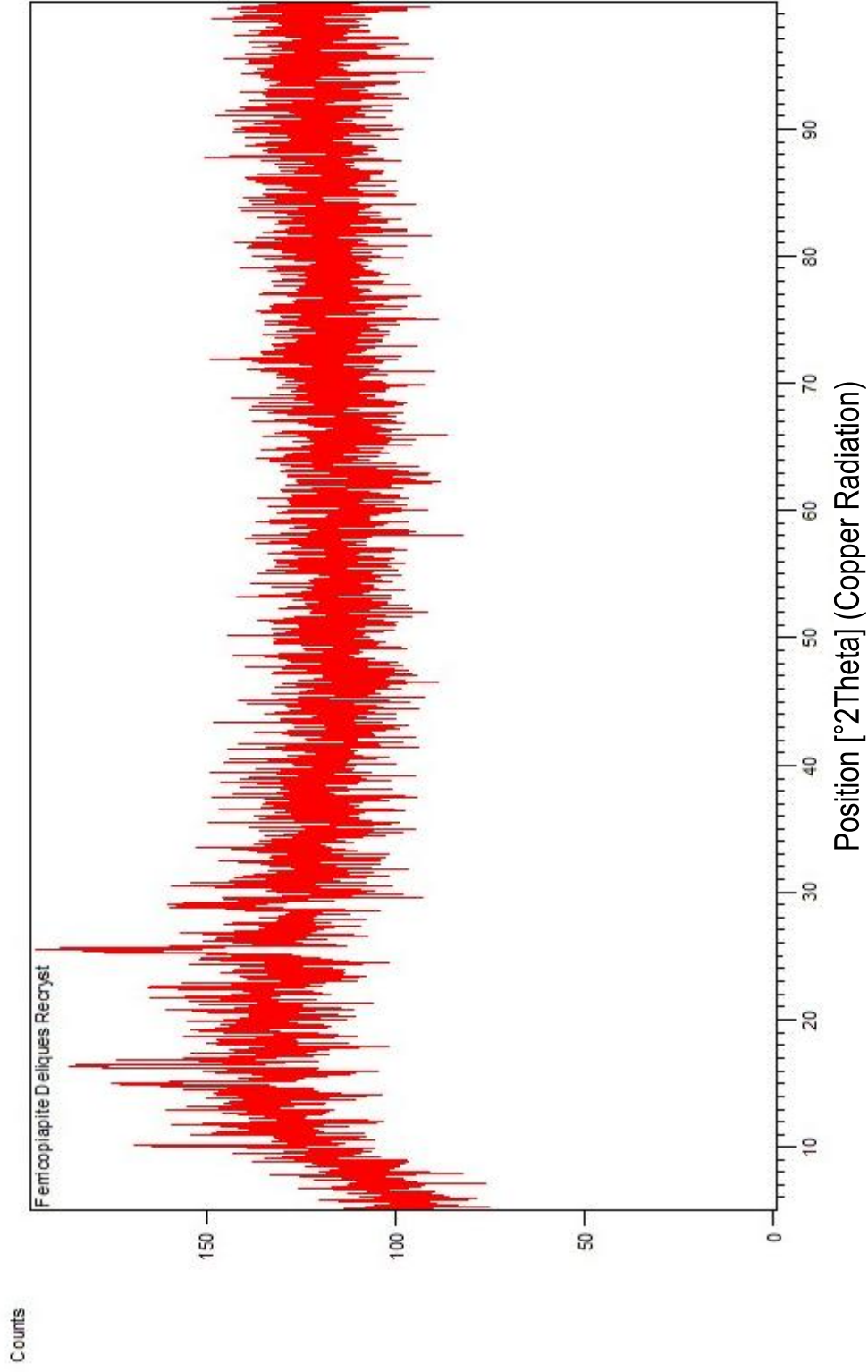


Figure 13 - XRD scan of ferricopiapite crust after deliquescence and re-precipitation. Peaks are at d-spacings [Å] of 8.6, 5.8, 5.4, 3.5 and 3.1.

### *Melanterite Deliquescence*

Humidity in the chamber was set to a point above melanterite stability by using pure water in the humidity buffer solution container. A single melanterite crystal was placed into the surface resistivity probe chamber with the wires touching the surface of the synthesized melanterite crystal. When the valve to the humidity buffer solution container was opened, the process was monitored and the deliquescence point recorded.

The change in relative humidity over time for the melanterite experiment are shown in Figure 14 and the deliquescence points for melanterite obtained in this experiment are shown in Figure 15 and Table 5, along with the values obtained in a previous study by Chou & Seal (2002).

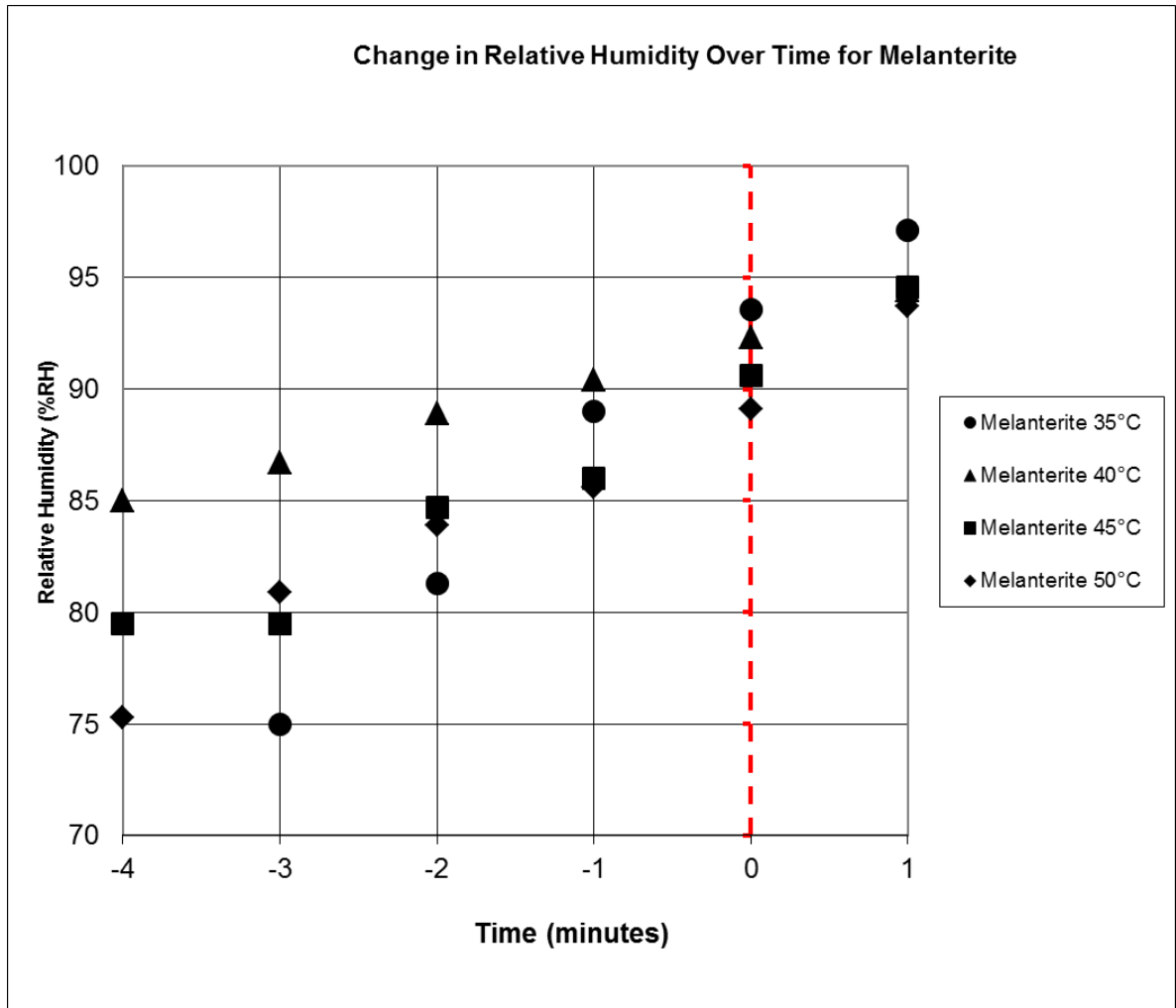


Figure 14 - Rates of increase of relative humidity for melanterite experiment.

Deliquescence occurs at zero minutes and is indicated by the dashed vertical line.

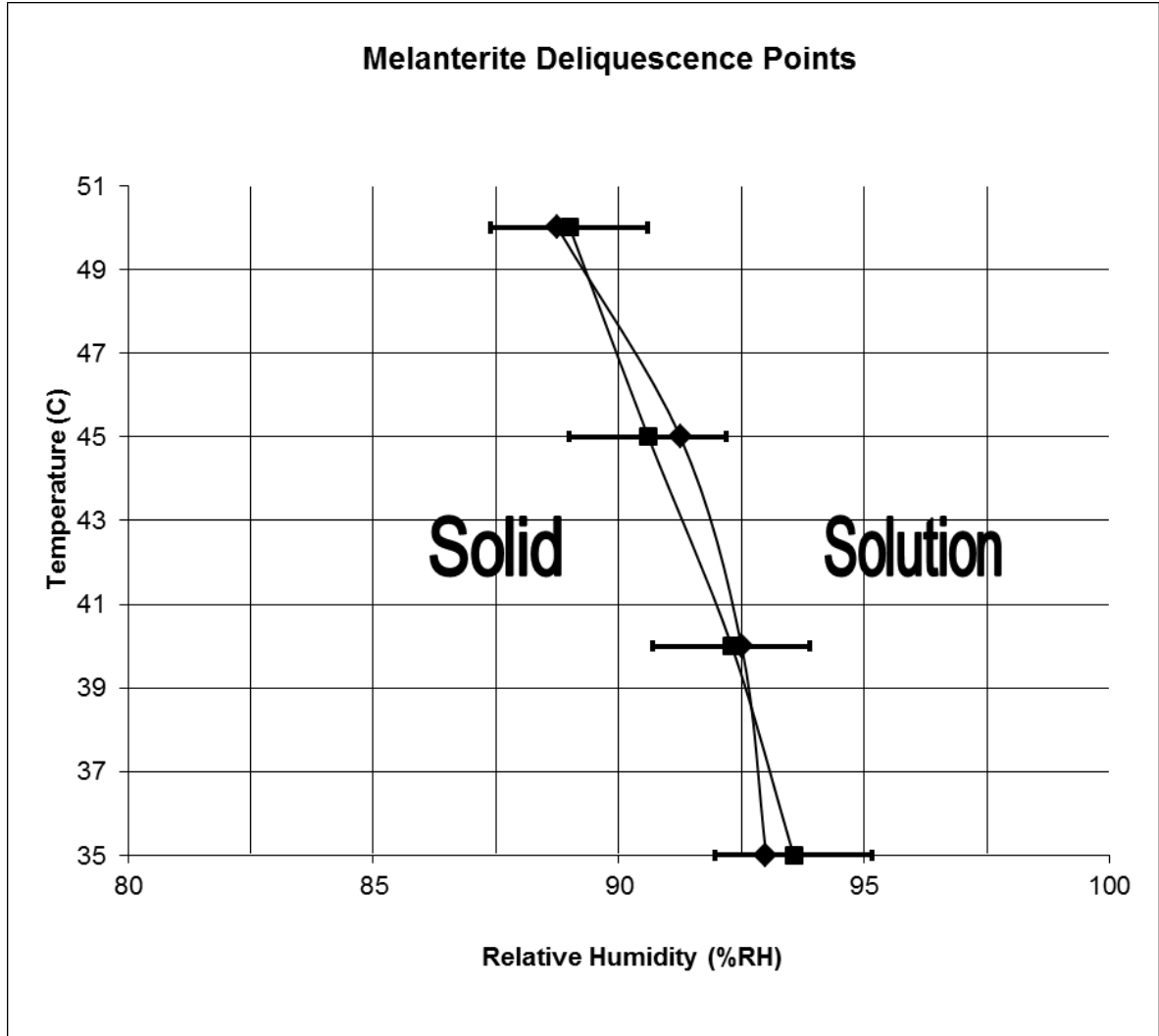


Figure 15 - Stability field of melanterite as a function of temperature and relative humidity. Filled diamonds are from Chou & Seal (2002), and filled squares are from this study. Error bars are for the values obtained in this study and are calculated from error for the Edgetech 2000 chilled mirror hygrometer and the Sensirion SHT 1x.

Temperature (°C)	Chou and Seal 2002 (%RH)	Deliquescence Humidity (%RH)
35	93	93.6 +/- 1.2
40	92.5	92.3 +/- 1.3
45	91.3	90.6 +/- 1.4
50	88.8	89.0 +/- 1.6

Table 5 - Deliquescence points for melanterite at various temperatures. Error was determined by propagating the error for the Edgetech 2000 chilled mirror hygrometer and the Sensirion SHT 1x through the formulae for calculation.

### *Halite Deliquescence*

Single crystals of halite were inserted into the surface resistivity probe chamber and the wires were positioned on the crystal surface. The relative humidity in the sample chamber was changed by adjusting the amount of dry air that was mixed with the humid air produced by the buffer solution. Pure water was used in the buffer chamber to increase the relative humidity range as much as possible. The change in relative humidity over time is presented in Figures 16, 17 and 18 while the deliquescence points obtained in this experiment are presented in Figure 19 and Table 6. The deliquescence points obtained for decreasing relative humidity agree with the values from Greenspan (1976).

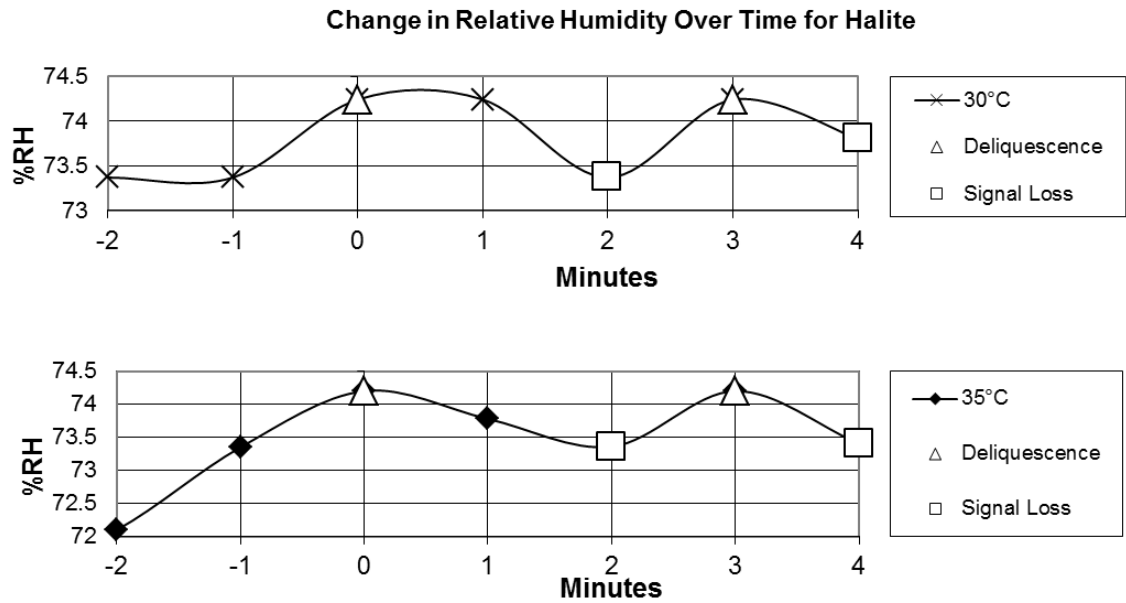


Figure 16 - Change in relative humidity over time for halite experiments at 30°C and 35°C. Each chart shows recorded values beginning at two minutes before initial deliquescence. Deliquescence is indicated by open triangles whereas loss of signal is indicated by open squares.

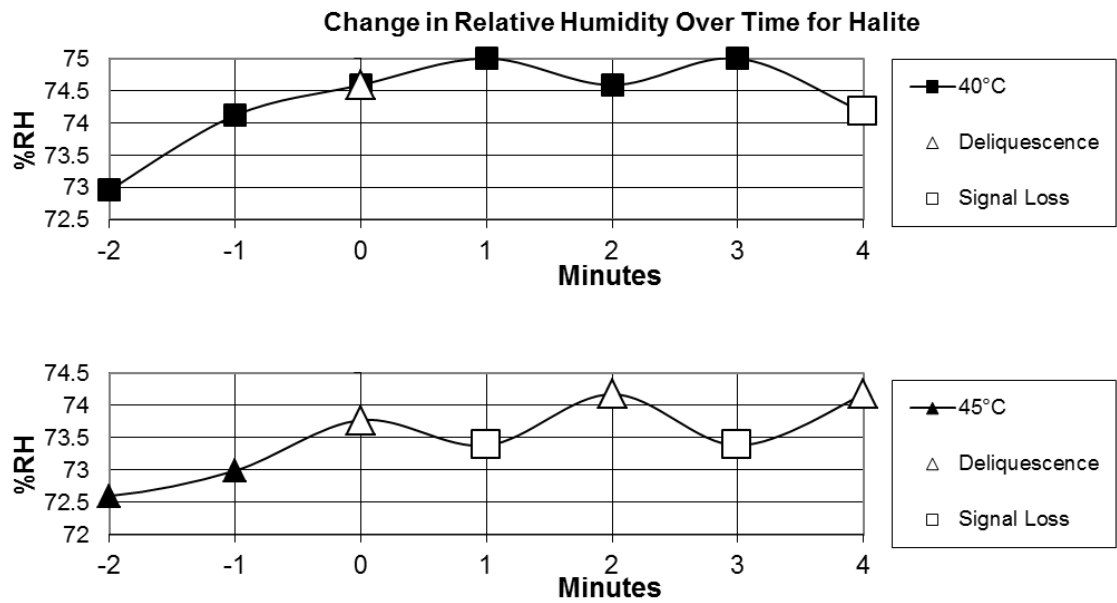


Figure 17 Change in relative humidity over time for halite experiments at 40°C and 45°C. Each chart shows recorded values beginning at two minutes before initial deliquescence. Deliquescence is indicated by open triangles whereas loss of signal is indicated by open squares.

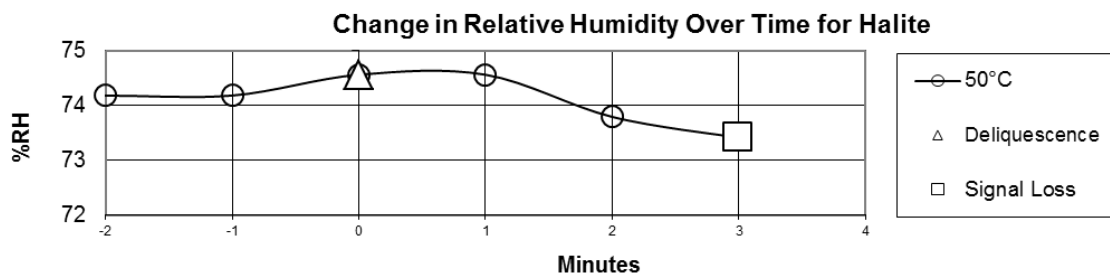


Figure 18 - Change in relative humidity over time for halite experiment at 50°C. Chart shows recorded values beginning at two minutes before initial deliquescence. Deliquescence is indicated by open triangles whereas loss of signal is indicated by open squares.

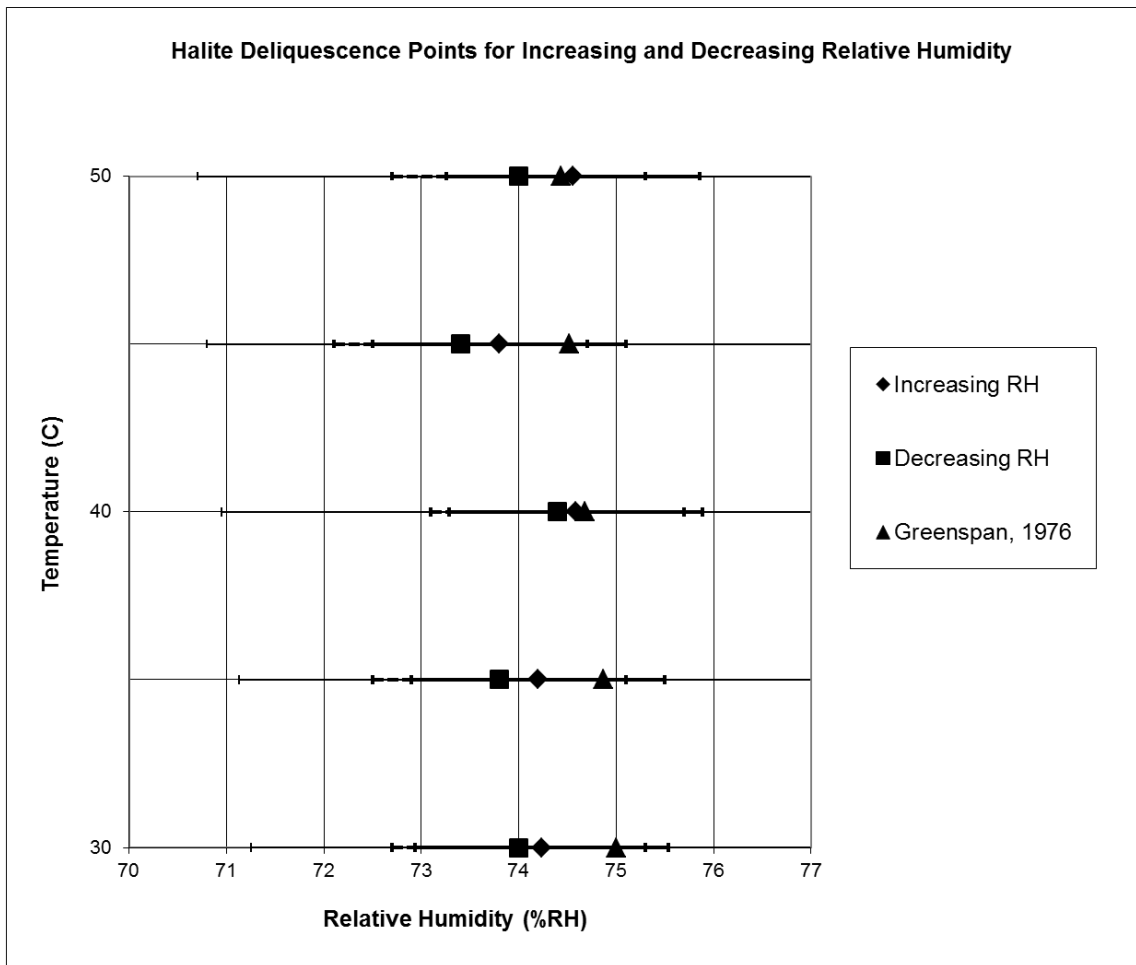


Figure 19 - Deliquescence points for halite. Values obtained from increasing relative humidity are indicated by diamonds while values obtained from decreasing relative humidity are shown as squares. Ideal values from Greenspan, 1976, are triangles. Error bars are for the values obtained in this study and are calculated from error for the Edgetech 2000 chilled mirror hygrometer and the Sensirion SHT 1x.

Temperature (°C)	Increasing Relative Humidity (%RH)	Decreasing Relative Humidity (%RH)	Ideal Humidities from Greenspan, 1976 (%RH)
30	74.2 +/- 1.1	74.0 +/- 1.1	75.1 +/-0.11
35	74.2 +/- 1.2	73.8 +/- 1.2	74.9 +/-0.12
40	74.6 +/- 1.3	74.4 +/- 1.3	74.7 +/-0.13
45	73.8 +/- 1.4	73.4 +/- 1.4	74.6 +/-0.16
50	74.6 +/- 1.6	74.0 +/- 1.6	74.4 +/-0.19

Table 6 - Deliquescence points obtained for halite using both increasing and decreasing relative humidity compared to ideal values taken from Greenspan (1976). Error for the values obtained in this study were determined by propagating the error for the Edgetech 2000 chilled mirror hygrometer and the Sensirion SHT 1x through the formulae for calculation.

## Epsomite Deliquescence

The deliquescence point for epsomite at various temperature and humidity values was required for study of the onset of deliquescence. The relative humidity above a liquid saturated with  $\text{MgSO}_4$  that is in equilibrium with  $\text{MgSO}_4 \cdot 7\text{H}_2\text{O}$  (epsomite), has been calculated previously by Chou & Seal (2003) and is shown in Figure 21. Because the values were calculated, an experiment was done to confirm the values. To create an epsomite buffer solution, epsomite was dissolved in distilled water until the solution was saturated at  $25^\circ\text{C}$ . Because the buffer solution only provided a known humidity when it was saturated with epsomite, additional epsomite was added to maintain saturation. This prevented under-saturation in the event of modest humidity sources or sinks (Greenspan, 1976). The solution was poured into a 125ml Nalgene™ bottle and inserted into the chamber in the buffer solution position as shown in Figure 9. Air flow to the surface resistivity probe chamber was shut off and the system measured the dew point above the buffer solution. The entire system was maintained at set

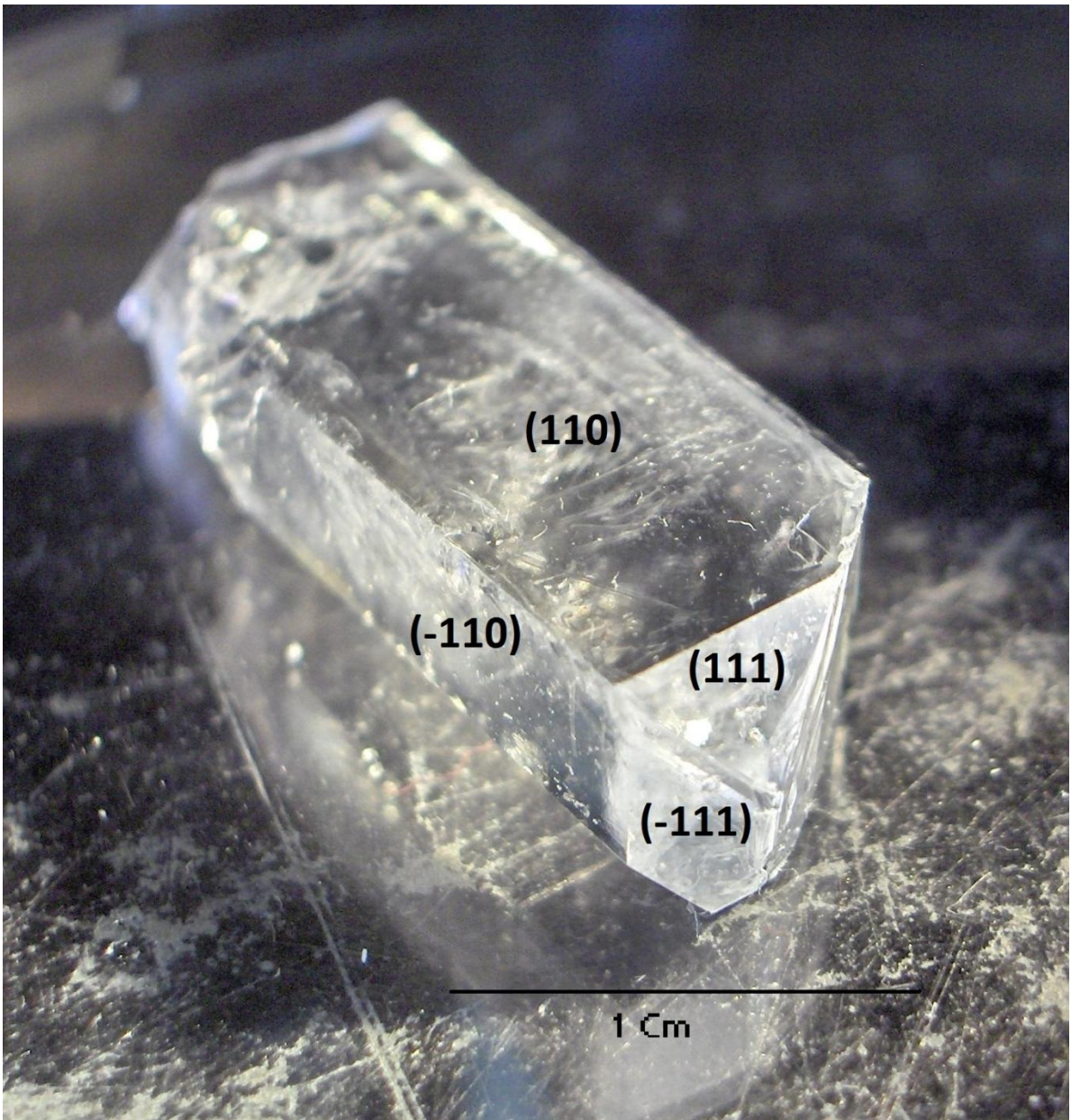


Figure 20 - Synthesized epsomite crystal. Faces are labeled with Miller indices.

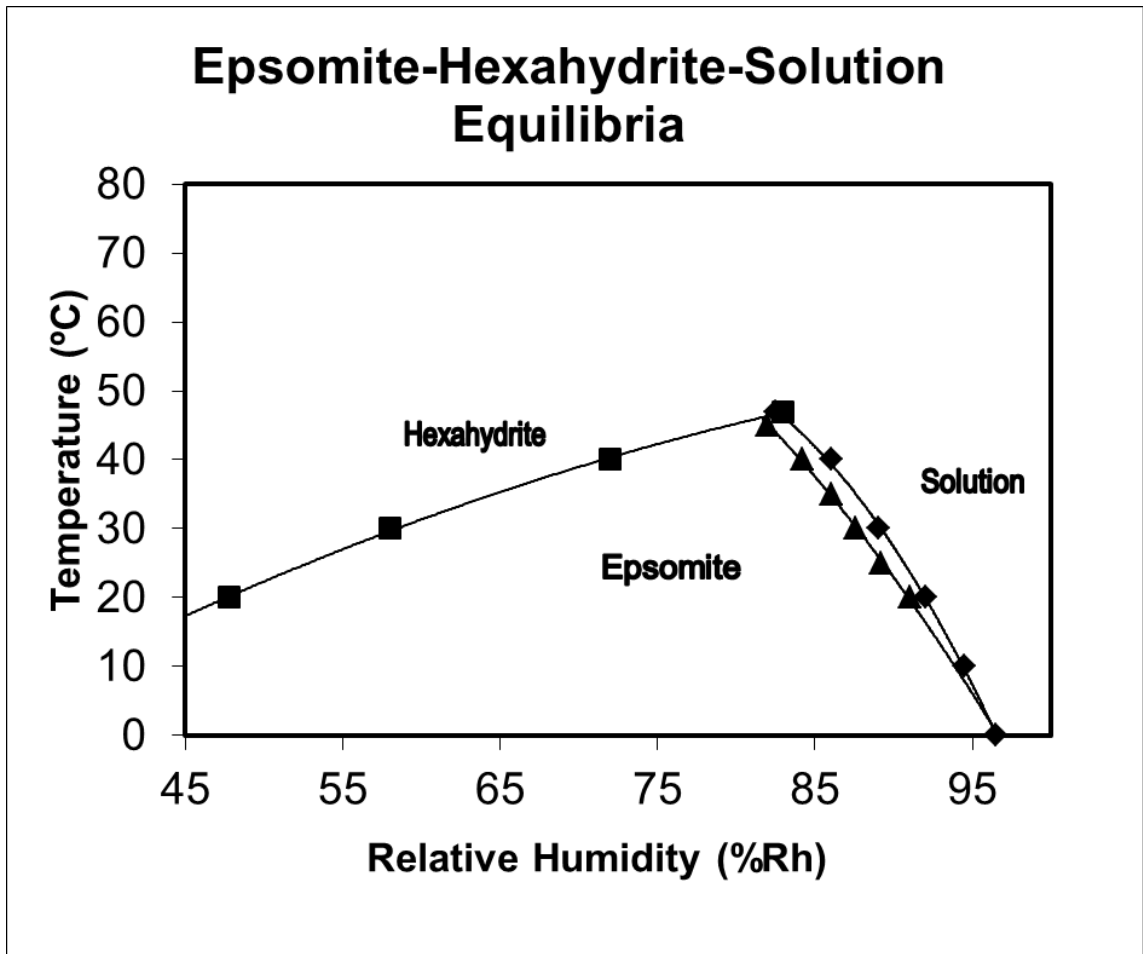


Figure 21 - Stability field of epsomite. The filled triangles are from this study.

The filled squares and triangles are experimental data from Chou & Seal (2003).

temperatures (30°C, 35°C, 40°C, 45°C, and 50°C). The solution was left for one day to allow for complete buffering of the air within the system and the humidity was measured by the Edgetech 2000. The relative humidity values observed for an epsomite solution in our study were on average 1-2% lower than those predicted by Chou & Seal (2003), but were within the error of our system.

Pairs of epsomite crystals were inserted into the surface resistivity probe chamber with one set of wires touching each crystal face of a different Miller index. The probe chamber was sealed and the temperature was allowed to equilibrate to the set value for the run. When the set temperature was achieved, the air valve to the surface resistivity probe chamber was opened, allowing the relative humidity to increase. The resistance across the surface of the crystals was monitored and the time at which a resistance other than infinite was measured was recorded. The buffer solution used was potassium sulfate which produced a relative humidity of 97.0% at 30°C (Greenspan, 1976). Several runs were performed at 20°C, 30°C, 35°C and 40°C, where the increase of relative humidity over time was great. One run was performed at a much slower increase in relative humidity over time. This was done to determine if one of the crystal faces had a lower deliquescence point or if there was indeed a difference in the onset of deliquesce at a maintained relative humidity. The relative humidity was increased to the point where the *l* face deliquesced, and then maintained at that value. The *m* face deliquesced at the same relative humidity as the *l* face; however, deliquescence occurred one hour and twenty seven minutes later.

Table 7 lists the beginning time of each experiment, and the time of deliquescence of both the *l* and the *m* face. As can be seen from Table 7 the *l* face was always the first to deliquesce. The time between deliquescence of the *l* and *m* face for the runs where the increase in relative humidity was rapid, ranged from as little as 21s to as much as 15m 9s.

Rapid Increase in Relative Humidity Over Time													
Run	Temp (°C)	Equilibrium Dewpoint Temp (°C)		Time of Deliquescence						Time Between Deliquescence of l and m Face		First to Deliquesce	
		l	m	Dewpoint	RH%	Error %RH	m	Dewpoint	RH%	Error %RH			
1	20	18.5	18.4	18.4	90.5	0.8	15:02:17	19.1	94.6	0.8		0:15:09	l
2	30	27.7	27.9	27.9	88.6	1.1	11:19:45	29.1	95.0	1.1		0:04:18	l
3	30	27.7	26.8	26.8	83.1	1.1	13:02:31	28.0	89.1	1.1		0:06:00	l
4	30	27.7	26.8	26.8	83.1	1.1	13:30:49	27.5	86.5	1.1		0:07:00	l
5	30	27.7	27.1	27.1	84.5	1.1	14:45:07	27.6	87.0	1.1		0:01:29	l
6	30	27.7	27.1	27.1	84.5	1.1	10:13:09	28.5	91.7	1.1		0:04:00	l
7	35	32.2	32.0	32.0	84.6	1.2	12:24:50	32.6	87.5	1.2		0:07:42	l
8	35	32.2	31.8	31.8	83.6	1.2	13:56:25	32.8	88.5	1.2		0:05:10	l
9	35	32.2	33.0	33.0	89.5	1.2	13:02:06	33.1	90.0	1.2		0:00:21	l
10	35	32.2	32.6	32.6	87.5	1.2	14:42:55	32.8	88.5	1.2		0:01:09	l
11	40	36.8	37.4	37.4	87.0	1.3	16:06:35	37.5	87.4	1.3		0:09:10	l
12	40	36.8	36.7	36.7	83.7	1.3	10:53:08	37.9	89.3	1.3		0:05:21	l
13	40	36.8	37.3	37.3	86.5	1.3	11:40:50	37.4	87.0	1.3		0:00:23	l
Slow Increase in Relative Humidity Over Time													
Run	Temp (°C)	Equilibrium Dewpoint Temp (°C)		Time of Deliquescence						Time Between Deliquescence of l and m Face		First to Deliquesce	
		l	m	Dewpoint	RH%	Error %RH	m	Dewpoint	RH%	Error %RH			
1	35	27.7	31.5	31.5	82.2	1.2	15:37:09	31.5	82.2	1.2		1:27:40	l

Table 7 – Results of the epsomite crystal face deliquescence experiments.

## Chapter 5: Discussion

### Ferricopiapite Deliquescence

The deliquescence point for ferricopiapite at various temperatures was determined using the surface resistivity probe chamber. The deliquescence points obtained in this experiment vary from 60.1% to 62.0% relative humidity in the range of 30°C to 50°C. The relative humidity at which ferricopiapite will deliquesce drops very slightly with increasing temperature. It was also shown that after allowing a sample of ferricopiapite to completely deliquesce and re-crystallize no ferricopiapite was present; however, there was a very small amount of crystalline material present that could not be readily identified.

The solid/solution boundary obtained in this study was compared to that of Chou & Seal (2002). Comparison solid/solution boundaries show agreement of the values within error. The agreement of the boundaries confirmed that the data obtained with the apparatus in this study is consistent with measurements made by others.

The halite deliquescence experiment obtained identical deliquescence points for both increasing and decreasing relative humidity. The data obtained validated the method used in the ferricopiapite crust and melanterite

deliquescence experiments. There was difficulty in obtaining the deliquescence point for a mineral by decreasing relative humidity as there was a period of time in which the sample would continue to deliquesce after it reached its deliquescence point. The longer it was allowed to deliquesce, the more solution evolved on the surface. More solution on the surface produced longer re-crystallization times when lowered below the deliquescence point, which introduced lag to the system. The melanterite and halite deliquescence experiments confirmed the method used to obtain the solid/solution boundary for ferricopiapite.

## Epsomite Deliquescence

The results of the crystal face deliquescence experiments clearly show that deliquescence occurred on the *l* face of epsomite crystals before it occurred on the *m* face. The difference in time for deliquescence to occur can be attributed to the difference in structure of the crystal surface between faces. The water molecules in the epsomite structure that co-ordinate the magnesium donate hydrogen bonds to the sulfate oxygens and a seventh water molecule located at the surface, or inside the crystal. The sulfate oxygens are all hydrogen bond acceptors (Fortes, 2005), and are thus able to make bonds with atmospheric water. Slices through the structure were produced to illustrate the possibility of an increased number of (w7) molecules and sulfate tetrahedra available on one face, slice, or plane of the structure over another. Figures 22

and 23 show cuts which are parallel to the *m* face of the epsomite crystal, while Figures 24 and 25 show a cut along the *l* face. The cuts were made where a surface could be produced with only the breaking of hydrogen bonds. The *l* face of the crystal was dominated by (w7) molecules and sulfate tetrahedra, whereas the *m* face consisted of magnesium octahedra and (w7) molecules.

The (w7) molecule was not coordinated to magnesium and was still able to form two additional hydrogen bonds with water in the atmosphere, it is also loosely bonded within the crystal structure and must be engaged less on the surface of the crystal than within the structure (Calleri et al., 1984). The oxygen molecules that were part of the sulfate tetrahedra were also able to form hydrogen bonds with atmospheric water. Because the oxygens in the sulfate tetrahedra have no hydrogens bonded to them, they would form hydrogen bonds with atmospheric water more readily than the oxygen atoms in the magnesium octahedral would.

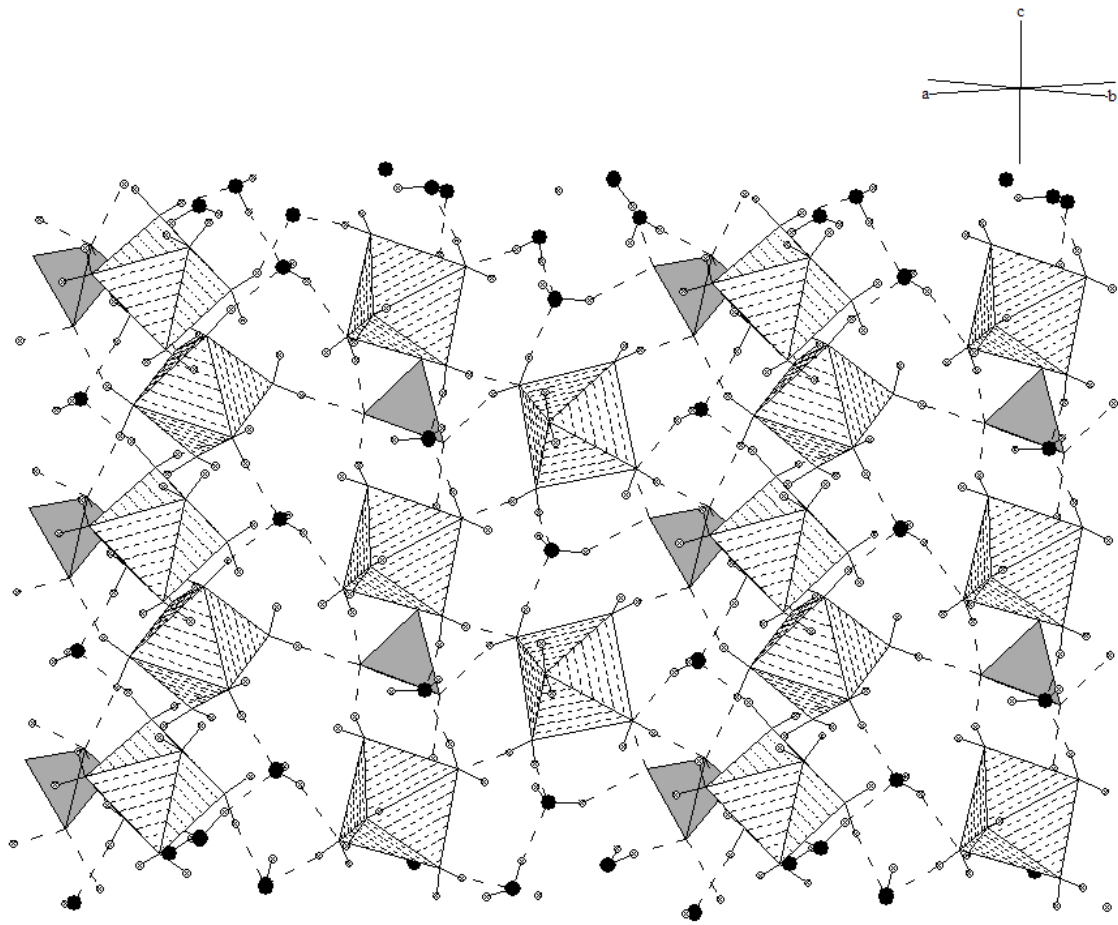


Figure 22 - Surface atoms for a particular slice along the  $m(110)$  face of epsomite as viewed  $45^\circ$  from the  $a$  and  $b$  axis. Black atoms are oxygen, checked atoms are hydrogen, dashed octahedra are magnesium and grey tetrahedra are sulfur (Calleri et al., 1984).

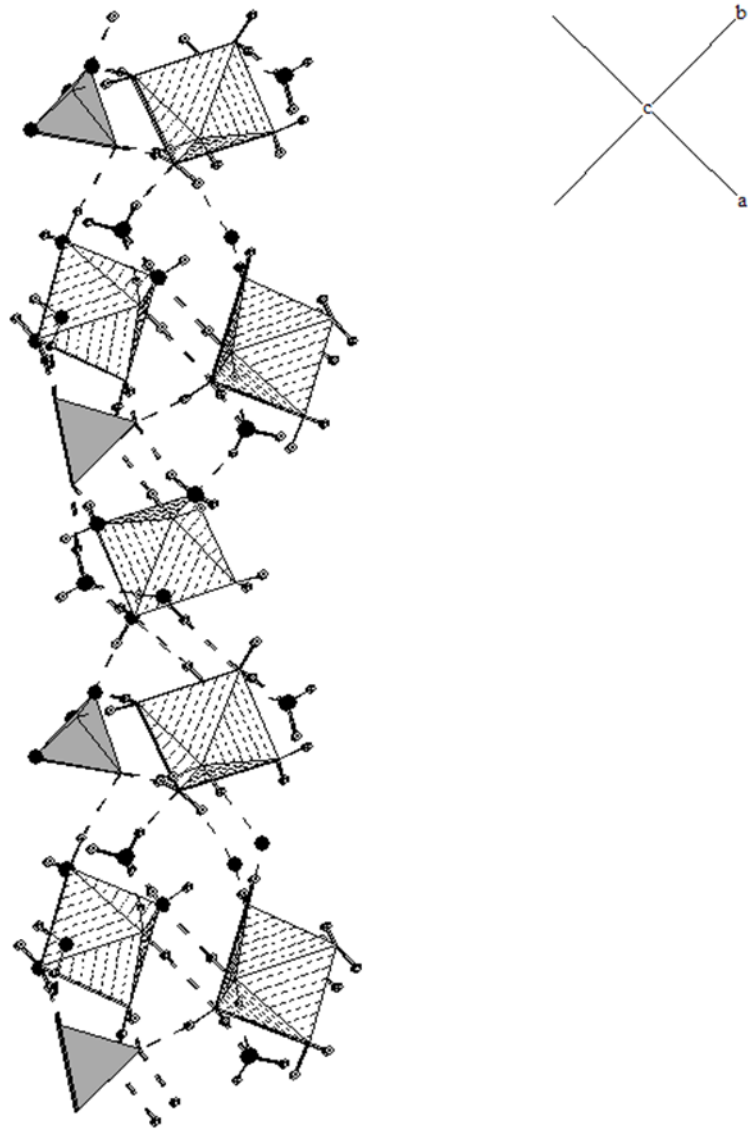


Figure 23 - Surface atoms for cross section of the  $m$  (110) face of epsomite as viewed down the  $c$  axis. Black atoms are oxygen, checked atoms are hydrogen, dashed octahedra are magnesium and grey tetrahedra are sulfur (Calleri et al., 1984).

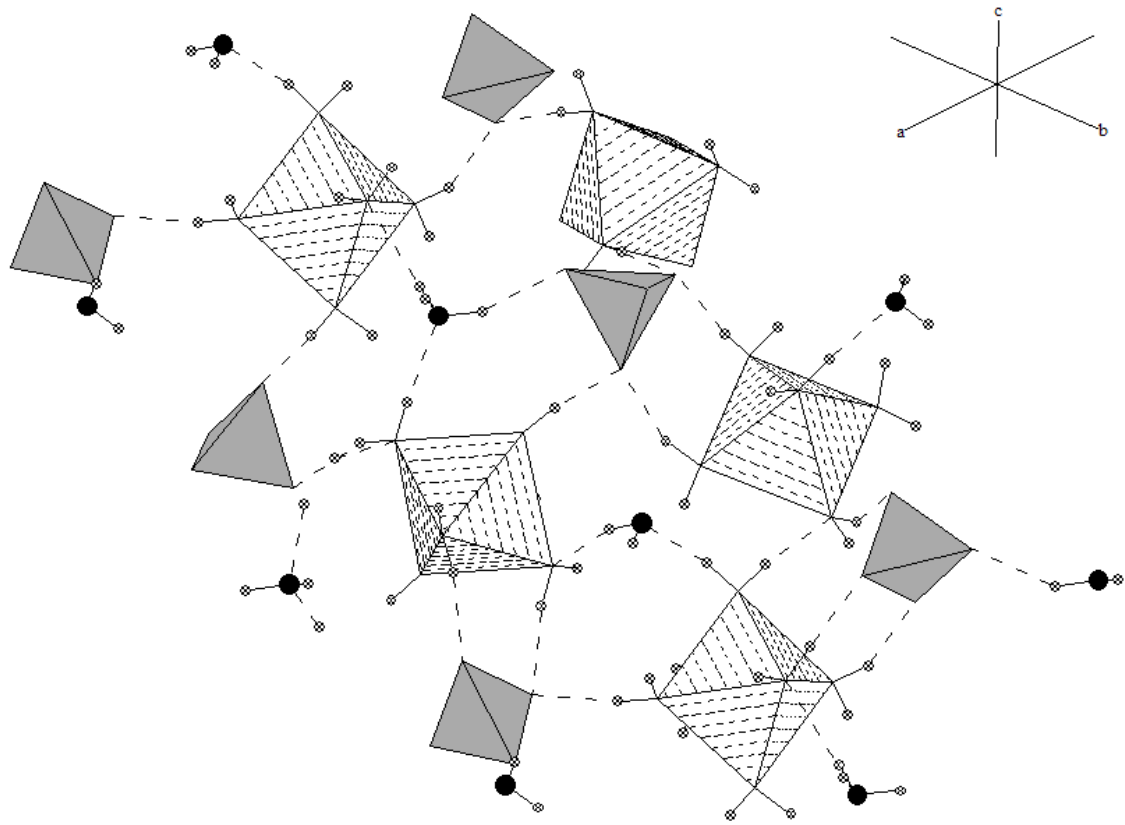


Figure 24 - Surface atoms for a particular slice, along the  $(111)$  face of epsomite as viewed perpendicular to the face. Black atoms are oxygen, checked atoms are hydrogen, dashed octahedra are magnesium and grey tetrahedra are sulfur (Calleri et al., 1984).

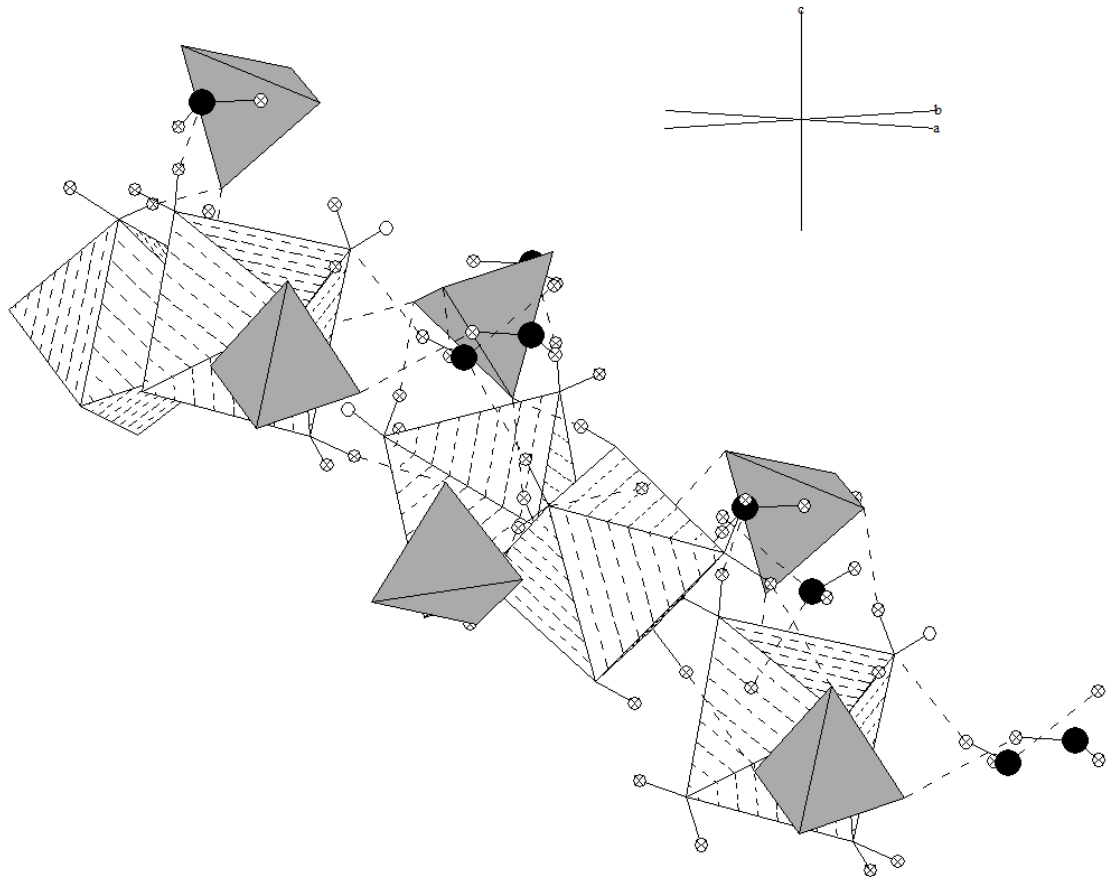


Figure 25 - Surface atoms for a particular slice, along the  $l(111)$  face of epsomite as viewed perpendicular to the  $c$  axis and  $45^\circ$  from the  $a$  and  $b$  axis. Black atoms are oxygen, checked atoms are hydrogen, dashed octahedra are magnesium and grey tetrahedra are sulfur (Calleri et al., 1984).

When the relative humidity of the system increased, the partial pressure of the system allowed the (w7) molecules and oxygens coordinated to the sulfate atoms to form hydrogen bonds with the atmospheric water molecules. Atmospheric water molecules continued to adhere to the crystal surface and to the water already on the surface. The result is the accumulation of enough water to begin the dissolution of the crystal. The difference between the number of (w7) molecules and sulfate tetrahedra on the *l* face over the *m* face allows for more water molecules to adhere to the surface and thus allows the deliquescence to proceed more readily. When the first atoms leave the epsomite structure and enter the solution being added to the surface, dissolution pits begin to form. An idealized diagram of a dissolution pit is shown in Figure 26. Once the pits formed, and a saturated solution was created, the normal phase relationship between saturated solution and solid prevails. The pH of the solution is slightly lower than 7.

Crystals can grow faster in some directions than in others (Zhang et al, 1990). It is therefore not surprising that they dissolve more easily in some directions than in others. One would predict, therefore, that the largest faces, or the slowest growing, would also be the slowest to dissolve. In the case of epsomite, the slowest growing face is *m* (Ruiz-Agudo et al., 2008). It was determined in our experiments that the *m* face was always the last to deliquesce.

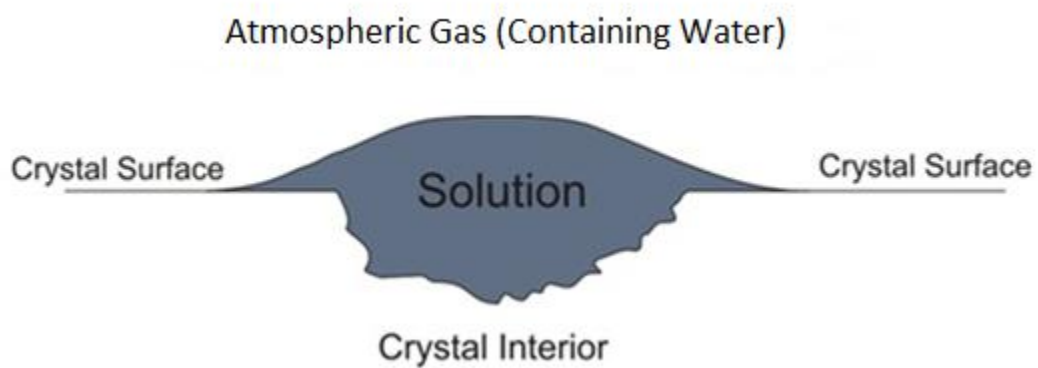


Figure 26 – Idealized diagram depicting dissolution pit formed on crystal surface upon initiation of deliquescence.

## Chapter 6: Conclusions

A temperature and humidity controlled chamber was constructed to allow the study of ferricopiapite deliquescence and the variation in the onset of deliquescence between mineral faces. The deliquescence point of ferricopiapite crust was studied. The data obtained from the melanterite and halite deliquescence experiments gave confidence in the data obtained during the ferricopiapite crust deliquescence experiment. The halite experiment also provided deliquescence points for decreasing relative humidity which were within 1.5% of the expected deliquescence humidity. The data obtained in this study allowed for the deliquescence points of ferricopiapite to be plotted against temperature and humidity.

Experiments were also conducted to observe the effects of deliquescence and subsequent recrystallization of ferricopiapite. The results showed that when a mineral deliquesces and the solution is allowed to evaporate, the mineral which precipitates out of that solution is not always the same as that which was initially deliquesced. When conducting deliquescence experiments the sample must not be allowed to deliquesce before study, as the mineralogy could change.

Finally, the difference in onset of deliquescence between faces of differing Miller indices was studied. It was shown that there is indeed a difference in the

onset of deliquescence between the faces. The *l* face first was always the first to deliquesce with the *m* face following at a later time.

Surface resistivity probes can only be used when there is a material that provides a solid, smooth surface between the two wires which are measuring resistivity. Materials on which the wire cannot maintain a connection with the surface of the material cannot be used. If powders are to be studied, they must be compressed into pellets in order to provide a solid surface for the probes to rest against. The solution which results from deliquescence can form a continuous layer on the surface of a mineral, which allows electrical current to flow and for a resistance to be measured.

## Future Work

Experiments could be conducted where relative humidity remains constant and the temperature is varied, such that the system being studied will move up and down through its deliquescence curve; however, the small dependence of deliquescence on temperature for some substances means that the relative humidity must be controlled very precisely. Further work can be performed at slower rates of increase of relative humidity to obtain more data relating to crystal face deliquescence. Experiments could also be performed where the relative humidity is maintained just below the deliquescence point of epsomite for very long periods of time. This will determine if there is a point where the *l* face will deliquesce, but the *m* face will not.

## References

- Adriano, D.C. (2001). *Trace Elements in Terrestrial Environments* (2<sup>nd</sup> ed.). New York: Springer-Verlag.
- Akcil, A. & Koldas, S. (2006). Acid Mine Drainage (AMD): causes, treatment and case studies. *Journal of Cleaner Production*, 14, 1139-1145.
- Anderson, J. L., Peterson, R.C. & Swainson, I.P. (2007). The Atomic Structure and Hydrogen Bonding of Deuterated Melanterite,  $\text{FeSO}_4 \cdot 7\text{D}_2\text{O}$ . *The Canadian Mineralogist*, 45, 457-469.
- Baur, W.H. (1964). On the crystal chemistry of salt hydrates. III. The refinement of the crystal structure of  $\text{FeSO}_4 \cdot 7\text{H}_2\text{O}$  (melanterite). *Acta Crystallographica*, 17, 1167 – 1174.
- Baur, W.H. (1964). On the crystal chemistry of salt hydrates. IV. The refinement of the crystal structure of  $\text{MgSO}_4 \cdot 7\text{H}_2\text{O}$  (epsomite). *Acta Crystallographica*, 17, 1361-1369.
- Calleri, M., Gavetti, A., Ivaldi, G. & Rubbo, M. (1984). Synthetic epsomite,  $\text{MgSO}_4 \cdot 7\text{H}_2\text{O}$ : absolute configuration and surface features of the complementary {111} forms. *Acta Crystallographica*, B40, 218-222.

- Chou, I-M. & Seal, R.R. (2002). Determination of melanterite-rozenite and chalcantite-bonattite equilibria by humidity measurements at 0.1 MPa. *American Mineralogist*, 87, 108-114.
- Chou, I-M. & Seal, R.R. (2003). Determination of epsomite-hexahydrate equilibria by the humidity-buffer technique at 0.1 MPa with implications for phase equilibria in the system MgSO<sub>4</sub>-H<sub>2</sub>O. *Astrobiology*, 3, 619-630.
- Dickson, A. G., Wesolowski, D.J., Palmer, D.A. & Mesmer, R.E. (1990). Dissociation constant of bisulfate ion in aqueous sodium chloride solutions to 250 °C. *Journal of Physical Chemistry*, 94, 7978-7985.
- Encyclopedia Britannica (2010, June 1<sup>st</sup>). *Deliquescence*. Retrieved June 1<sup>st</sup>, 2010, from <http://www.britannica.com/EBchecked/topic/156605/deliquescence>
- Fortes, A. D., Wood, I., G., Alfredsson, M., Vočadlo, L. & Knight, K., S. (2005). The thermoelastic properties of MgSO<sub>4</sub>·7H<sub>2</sub>O (epsomite) from powder neutron diffraction and *ab initio* calculation. *European Journal of Mineralogy*, 18, 449-462.

- Frau, F., (2000). The formation-dissolution-precipitation cycle of melanterite at the abandoned pyrite mine of Genna Luas in Sardinia, Italy: environmental implications. *Mineralogical Magazine*, 64 (6), 995-1006.
- Friedlander, L. R., Tosca, N. J. & Arvidson, R. E. (2007). Preliminary experiments in the systematic investigation of the spectroscopic properties of synthetic copiapite group minerals. *Lunar and Planetary Science XXXVIII*, 2049.
- Gaines, R. V., Skinner, H.C.W., Foord, E.E., Mason, B., Rosenweig, A. & King, V.T. (1997). *Dana's New Mineralogy*. John Wiley & Sons Incorporated.
- Greenspan, L. (1976). Humidity fixed points of binary saturated aqueous solutions. *Journal of Research*, 81A (1), 89-96.
- Haüy, R. J. (1823). *Traité de mineralogy* (2<sup>nd</sup> ed.). Paris: Bachelier, Libraire.
- Jameson, L.A. (2007). An Investigation of the Stability Fields of the Hexahydrite and Rozenite Groups of Minerals with Melanterite Group Crystal Structure. *Undergraduate Thesis*, Queen's University.

Jamieson, H. E., Robinson, C., Alpers C.N., McCleskey, R.B., Nordstrom, D.K. & Peterson, R.C. (2005). Major and trace element composition of copiapite-group minerals and coexisting water from the Richmond mine, Iron Mountain, California. *Chemical Geology*, 215, 387-405.

Majzlan, J. & Michallik, R. (2007). The crystal structures, solid solutions, and infrared spectra of copiapite-group minerals. *Mineralogical Magazine*, 71 (5), 553-569.

Majzlan, J., Navrotsky, A., McCleskey, R., B. & Alpers, N. (2006). Thermodynamic properties and crystal structure refinement of ferricopiapite, coquimbite, rhomboclase, and  $\text{Fe}_2(\text{SO}_4)_3(\text{H}_2\text{O})_5$ . *European Journal of Mineralogy*, 18, 175-186.

Nation Physical Laboratory (2007, October 8<sup>th</sup>). *How do I convert between units of dew point and relative humidity? (FAQ - Thermal)*. Retrieved June 5<sup>th</sup>, 2010, from [http://www.npl.co.uk/engineering-measurements/thermal/temperature/faqs/how-do-i-convert-between-units-of-dew-point-and-relative-humidity-\(faq-thermal\)](http://www.npl.co.uk/engineering-measurements/thermal/temperature/faqs/how-do-i-convert-between-units-of-dew-point-and-relative-humidity-(faq-thermal))

Parallax Incorporated (2010, May 14<sup>th</sup>). *Board of Education® - USB (#28850)*. Retrieved June 1<sup>st</sup>, 2010, from <http://www.parallax.com/dl/docs/prod/boards/BOE-RevC-v1.3.pdf>

Parallax Incorporated (2005, April). *Stamp Specifications*. Retrieved June 1<sup>st</sup>, 2010, from [http://www.parallax.com/detail.asp?product\\_id=BS2-IC](http://www.parallax.com/detail.asp?product_id=BS2-IC), Basic Stamp 2

Plummer, L.N., Parkhurst, D.L., Fleming, G.W. & Dunkle, S.A. (1988). A Computer Program Incorporating Pitzer's Equations for Calculation of Geochemical Reactions in Brines. *U.S. Geological Survey Water-Resources Investigation Report*, 88–4153.

Posnjak, E. & Merwin, H. E. (1922). The system,  $\text{Fe}_2\text{O}_3\text{—SO}_3\text{—H}_2\text{O}$ . *Journal of the American Chemical Society*, 44(9), 1965-1994.

Ruiz-Agudo, E., Putnis, C.V. & Rodriguez-Navarro, C. (2008). Interaction between Epsomite Crystals and Organic Additives. *Crystal Growth and Design*, 8 (8), 2665-2673.

Sensirion Incorporated (2010, May). *Datasheet Sht 1x*. Retrieved June 1<sup>st</sup>, 2010, from [http://www.sensirion.com/en/pdf/product\\_information/Data\\_Sheet\\_humidity\\_sensor\\_SHT1x\\_SHT7x\\_E.pdf](http://www.sensirion.com/en/pdf/product_information/Data_Sheet_humidity_sensor_SHT1x_SHT7x_E.pdf)

- Steiger, M., Linnow, K., Erhardt, D. & Rohde, M. (n.d.). Decomposition reactions of magnesium sulfate hydrates and phase equilibria in the  $\text{MgSO}_4\text{-H}_2\text{O}$  and  $\text{Na}^+\text{-Mg}^{2+}\text{-Cl-}\text{SO}_4^{2-}\text{-H}_2\text{O}$  systems with implications for Mars.
- Vaniman, D.T. & Chipera, S.J., (2006). Transformations of Mg- and Ca-sulfate hydrates in Mars regolith. *American Mineralogist*, 91, 1628-1642.
- Young, R.A. (1995). *The Rietveld Method*. Oxford: Oxford English Press.
- Zhang, G., Kinoshita, T. & Sasaki, K. (1990). Crystal growth of 4-Br-4'-methoxychalcone and its characterization. *Journal of Crystal Growth*, 100, 411-416.
- Zodrow, E.L. & McCandlish, K. (1978). Hydrated sulfates in the Sydney coalfield, Cape Breton, Nova Scotia. *Canadian Mineralogist*, 16, 17-22.

## Appendix A

Structural data for ferricopiapite crust from Rietveld refinement.

### Global Parameters

Number of used phases	1
Number of variables	18
Number of constraints	0
Zero shift/ °2Theta	-0.0552(6)
Specimen displacement/ mm	0.000000
Profile function	Pseudo Voigt
Background	Polynomial
R (expected)/ %	2.36769
R (profile)/ %	3.61861
R (weighted profile)/ %	6.02323
GOF	6.47154
d-statistic	0.78023
U standard	0.000000
V standard	0.000000
W standard	0.010000

## Relevant parameters of 156227-ICSD

### Structure and profile data

Formula sum  $\text{Fe}_{4.63}\text{S}_{6.00}\text{O}_{46.00}\text{D}_{42.00}$

Formula mass/ g/mol 1271.7350

Density (calculated)/ g/cm<sup>3</sup> 2.2251

F(000) 584.4580

Weight fraction/ % 100.000000

Space group (No.) P -1 (2)

### Lattice parameters

a/ Å 7.3126(9)

b/ Å 7.372(1)

c/ Å 18.332(1)

alpha/ ° 98.911(9)

beta/ ° 93.937(9)

gamma/ ° 102.22(1)

V/ 10<sup>6</sup> pm<sup>3</sup> 948.90960

Overall displacement parameter 0.0(7)

Extinction -0.000007(1)

Flat Plate Absorption Correction 0.000000

Porosity 0.000000

Roughness 0.000000

Fitting mode Structure Fit

U 0.20(2)

V	-0.061(6)
W	0.0078(3)
Pref. orientation direction/ hkl	0.00 0.00 1.00
Pref. orientation parameter	0.635(5)
Asymmetry parameter 1	0.000000
Asymmetry parameter 2	0.000000
Peak shape	
parameter 1	0.54(2)
parameter 2	0.000000
parameter 3	0.000000
R (Bragg)/ %	3.91672

### Occupancy, atomic fract. coordinates and Biso for 156227-ICSD

Atom	Wyck	s.o.f.	x	y	z	Biso/ 10 <sup>4</sup> pm <sup>2</sup>
Fe1	1d	0.6	0.5	0.0	0.0	0.5
Fe2	2i	1.0	0.1	0.8	0.3	0.5
Fe3	2i	1.0	0.7	0.4	0.3	0.5
S1	2i	1.0	0.3	0.2	0.3	0.5
S2	2i	1.0	0.3	0.2	0.6	0.5
S3	2i	1.0	0.3	0.4	0.8	0.5
O1	2i	1.0	0.4	0.3	0.3	0.5

O2	2i	1.0	0.2	0.3	0.2	0.5
O3	2i	1.0	0.1	0.0	0.3	0.5
O4	2i	1.0	0.4	0.1	0.2	0.5
O5	2i	1.0	0.4	0.4	0.6	0.5
O6	2i	1.0	0.2	0.2	0.5	0.5
O7	2i	1.0	0.2	0.1	0.6	0.5
O8	2i	1.0	0.4	0.1	0.6	0.5
O9	2i	1.0	0.7	0.6	0.1	0.5
O10	2i	1.0	0.6	0.5	0.2	0.5
O11	2i	1.0	0.4	0.2	0.8	0.5
O12	2i	1.0	0.1	0.3	0.8	0.5
O13	2i	1.0	0.0	0.5	0.7	0.5
O14	2i	1.0	0.3	0.7	0.3	0.5
O15	2i	1.0	0.2	0.9	0.4	0.5
O16	2i	1.0	0.4	0.8	0.1	0.5
O17	2i	1.0	0.7	0.3	0.4	0.5
O18	2i	1.0	0.2	0.1	1.0	0.5
O19	2i	1.0	0.8	0.2	0.3	0.5
O20	2i	1.0	0.5	0.2	0.1	0.5
O21	2i	1.0	0.1	0.2	0.1	0.5
O22	2i	1.0	0.2	0.5	0.4	0.5
O23	2i	1.0	0.1	0.6	0.1	0.5

D1	2i	1.0	0.0	0.5	0.4	0.5
D2	2i	1.0	0.4	0.7	0.3	0.5
D3	2i	1.0	0.2	0.6	0.3	0.5
D4	2i	1.0	0.6	0.1	0.6	0.5
D5	2i	1.0	0.8	0.0	0.6	0.5
D6	2i	1.0	0.3	0.7	0.1	0.5
D7	2i	1.0	0.5	0.7	0.1	0.5
D8	2i	1.0	0.7	0.2	0.4	0.5
D9	2i	1.0	0.3	0.6	0.5	0.5
D10	2i	1.0	0.2	0.1	0.0	0.5
D11	2i	1.0	0.9	0.1	0.0	0.5
D12	2i	1.0	0.9	0.2	0.3	0.5
D13	2i	1.0	0.7	0.0	0.3	0.5
D14	2i	1.0	0.6	0.3	0.1	0.5
D15	2i	1.0	0.5	0.2	0.1	0.5
D16	2i	1.0	0.1	0.3	0.1	0.5
D17	2i	1.0	0.1	0.3	0.1	0.5
D18	2i	1.0	0.2	0.3	0.5	0.5
D19	2i	1.0	0.3	0.5	0.4	0.5
D20	2i	1.0	0.0	0.5	0.1	0.5
D21	2i	1.0	0.1	0.7	0.1	0.5

## Appendix B

Structural data for melanterite from Rietveld refinement.

### Global Parameters

Number of used phases	1
Number of variables	11
Number of constraints	0
Zero shift/ °2Theta	-0.164(4)
Specimen displacement/ mm	0.000000
Profile function	Pseudo Voigt
Background	Polynomial
R (expected)/ %	2.42573
R (profile)/ %	4.09375
R (weighted profile)/ %	8.34513
GOF	11.83539
d-statistic	0.25025
U standard	0.000000
V standard	0.000000
W standard	0.010000

## Relevant parameters of 55320-ICSD

### Structure and profile data

Formula sum	Fe <sub>4.00</sub> S <sub>4.00</sub> O <sub>44.00</sub>
Formula mass/ g/mol	1055.6020
Density (calculated)/ g/cm <sup>3</sup>	1.8052
F(000)	520.0000
Weight fraction/ %	100.000000
Space group (No.)	P 1 21/c 1 (14)

### Lattice parameters

a/ Å	14.055(3)
b/ Å	6.498(1)
c/ Å	11.040(3)
alpha/ °	90
beta/ °	105.662(9)
gamma/ °	90
V/ 10 <sup>6</sup> pm <sup>3</sup>	970.85370
Overall displacement parameter	10(1)
Extinction	0.000000
Flat Plate Absorption Correction	0.000000
Porosity	0.000000
Roughness	0.000000
Fitting mode	Structure Fit
U	0.000000

V	0.000000
W	0.0053(3)
Pref. orientation direction/ hkl	0.00 0.00 1.00
Pref. orientation parameter	1.000000
Asymmetry parameter 1	0.000000
Asymmetry parameter 2	0.000000
Peak shape	
parameter 1	0.600000
parameter 2	0.000000
parameter 3	0.000000
R (Bragg)/ %	14.46682

### Occupancy, atomic fract. coordinates and Biso for 55320-ICSD

Atom	Wyck	s.o.f.	x	y	z	Biso/ 10 <sup>4</sup> pm <sup>2</sup>
Fe1	2b	1.0	0.5	0.0	0.0	1.7
Fe2	2c	1.0	0.0	0.0	0.5	1.7
S1	4e	1.0	0.3	0.0	0.3	1.5
O1	4e	1.0	0.3	0.0	0.5	2.3
O2	4e	1.0	0.6	0.5	0.2	2.4
O3	4e	1.0	0.8	0.4	0.2	2.4
O4	4e	1.0	0.2	0.2	0.3	2.6

O5	4e	1.0	0.4	0.1	0.1	4.1
O6	4e	1.0	0.6	0.0	0.2	2.7
O7	4e	1.0	0.5	0.2	0.4	2.4
O8	4e	1.0	0.0	0.0	0.3	2.5
O9	4e	1.0	0.1	0.2	0.1	2.6
O10	4e	1.0	0.1	0.6	0.1	2.6
O11	4e	1.0	0.1	0.5	0.4	2.8

## Appendix C

### Edgetech 2000™ Hygrometer Specifications

#### Dew/Frost Point Range

- 40 to +100°C (-40 to 212°F) - S1, Ds1 Sensor -50 to +100°C (-50 to 212°F)
  - S2, Ds2 Sensor
- 75 to +100°C (-103 to 212°F) - S3 Sensor

#### Accuracy

- Dew point/Frost                       $\pm 0.2^{\circ}\text{C}$  ( $\pm 0.36^{\circ}\text{F}$ )
- Ambient Temperature\*             $\pm 0.2^{\circ}\text{C}$  ( $\pm 0.36^{\circ}\text{F}$ )
- Relative Humidity\*                0.5%RH, nominal

#### Dew/Frost Point Temperature Sensor

- 3-wire Platinum Resistance Thermometer (PRT), 100 ohms at 0°C,  
nominal

#### Depression

- 45°C (81°F), nominal - S1, Ds1 Sensor
- 65°C (117°F), nominal - S2, Ds2 Sensor
- 95°C (171°F), nominal - S3 Sensor

### **Relative Humidity Range**

- 5 to 100%, nominal -S1
- Ds1 Sensor 1 to 100%, nominal - S2
- Ds2 Sensor <1 to 100%, nominal - S3

### **Ambient Temperature Range**

- 50 to 130°C (-58 - 266°F)

### **Auxiliary Coolant**

- Water (or other) - 2 liters/minute (0.5 gallon/ minute) at 100 psig maximum, to augment depression capability of Sensor when necessary.
- S1 Sensor - Coolant port standard S2 Sensor - Coolant port standard

### **Sensor Material**

- Rhodium or Nickel Chromium mirror, glass, epoxy, isofoam insulation, anodized aluminum sensor body.

### **Depression Slew Rate**

- 1.7°C (3°F)/second max., above 0°C

**Repeatability**

- $\pm 0.01^{\circ}\text{C}$  ( $0.2^{\circ}\text{F}$ )

**Hysteresis**

- None

**Sample Flow Rate**

- 0.25-2.5 liters/minute (0.5-5.0 SCFH)

**Sample Pressure**

- 0-21 kg/cm<sup>2</sup> (0-300 psia) - S1, S2, S3
- 0-63 kg/cm (0-900 psia) - S1P, S2P

**Operating Temperature**

- 0 to 50°C (32 to 122°F) - Control Unit -50 to 70°C (-58 to 158°F) - S1  
Sensor
- 50 to 100°C (-58 to 212°F) - S2 Sensor -75 to 75°C (-103 to 167°F) - S3  
Sensor

**Display**

- 4-digit LED alphanumeric data display
- 0.6 in. high digits
- 0.1°C/0.1°F resolution, (-) XXX.X C/F

## Keypad

- 16 keys, to provide programming for Model 2000 Series functions:
  - °C/°F toggle
  - View/change time, date, digital averaging, baud rate
  - Manual Auto Balance Control initiate
  - Programmable Auto Balance Control for start time, interval, output
  - Track/Hold
  - Maximum Heat toggle Maximum Cool toggle
  - View/change high and low limits for analog outputs
  - View/change Alarm parameters - high/low limits, high and/or low alarms, latched or unlatched relays
  - Reset front panel Alarm indicators (latched only)

## Outputs

- Track or Hold
- Outputs (analog, digital, alarms) can be set or Track or Hold while in Auto Balance or Programming mode.

## Analog

- Voltage (Standard)
- 0 to 5 VDC, scalable from -100 to 100°C (-148 to 212°F), 1K minimum impedance

## **Current**

### Internal or External Power (Standard)

- 4 to 20 ma, scalable from -100 to 100°C (-148 to 212°F), 1000 ohms maximum loop resistance Isolated (Optional)
- 4 to 20 ma, scalable from -100 to 100°C (-148 to 212°F), 1000 ohms maximum loop resistance

## **Digital**

### RS-232

- 300/1200/2400/4800/9600/192000 Baud N81 25-pin D-subminiature connector (female). Output of time and dew/frost point, output intervals, plus on-line Help menu.

## **Mirror Condition (Contaminated)**

Rear panel TTL output and front panel LED

## **Two Alarms**

- Two Form C, SPDT alarm relays rated for 3 amps at 24 VDC, 120 VAC
- Alarm mode (high and low) programmable from keypad or RS-232
- Alarm set point programmable from -99.9 to 99.9°C (-148 to 212°F) from keypad or RS-232 port.
- Alarms can be latched or unlatched.

### **Auto Balance Control**

- Manual initiate of ABC at any time.
- Automatic ABC with start time and interval programmable from keypad or RS-232 port.
- Outputs programmable for Track or Hold during ABC.

### **Weight**

- 7.0kg (15.5 pounds), desk-top version
- Rack mount available

### **Dimensions**

- 28.2 (W) x 13.0 (H) x 45.7 (D) cm (11.1 (W) x 5.1 (H) x 18 (D) in.), desk-top with S2 Sensor mounted.

### **Mounting**

- Desk-top (standard)
- Panel/Rack (optional)
- NEMA 4 Enclosure (optional)

### **Power Requirements**

- 100/115/230 VAC,  $\pm 10\%$ , 50-60 Hz,
- 75 watts maximum

## **Fuses**

- 240 VAC Operation - 1A, 3AG, 250 VAC, Slo-Blo
- 120 VAC Operation - 2A, 3 AG, 250 VAC, Slo-Blo

## Appendix D

### Technical data for Basic Stamp 2™ module

**Stamp Specifications (revised 04/05)**

Released Products	Rev.Dx / BS1HC		BS2-IC		BS2e-IC		BS2sx-IC	
	PCB w/Proto / 14-pin SIP	24-pin DIP	24-pin DIP	24-pin DIP	24-pin DIP	24-pin DIP	24-pin DIP	24-pin DIP
Package	2.5" x 1.5" x .5" / 1.4" x .6" x .1"	1.2" x 0.6" x 0.4"	1.2" x 0.6" x 0.4"	1.2" x 0.6" x 0.4"	1.2" x 0.6" x 0.4"	1.2" x 0.6" x 0.4"	1.2" x 0.6" x 0.4"	1.2" x 0.6" x 0.4"
Environment *	0° - 70° C (32° - 158° F) **	0° - 70° C (32° - 158° F) **	0° - 70° C (32° - 158° F) **	0° - 70° C (32° - 158° F) **	0° - 70° C (32° - 158° F)	0° - 70° C (32° - 158° F)	0° - 70° C (32° - 158° F)	0° - 70° C (32° - 158° F)
Microcontroller	Microchip PIC16C56a	Microchip PIC16C57c	Microchip PIC16C57c	Ubicom SX28AC	Ubicom SX28AC	Ubicom SX48AC	Ubicom SX48AC	Ubicom SX48AC
Processor Speed	4 MHz	20 MHz	20 MHz	20 MHz	20 MHz	25 MHz Turbo	25 MHz Turbo	25 MHz Turbo
Program Execution Speed	~2,000 instructions/sec.	~4,000 instructions/sec.	~4,000 instructions/sec.	~4,000 instructions/sec.	~4,000 instructions/sec.	~19,000 instructions/sec.	~19,000 instructions/sec.	~8,500 instructions/sec.
RAM Size	16 Bytes (2 I/O, 14 Variable)	32 Bytes (6 I/O, 26 Variable)	32 Bytes (6 I/O, 26 Variable)	32 Bytes (6 I/O, 26 Variable)	32 Bytes (6 I/O, 26 Variable)	32 Bytes (6 I/O, 26 Variable)	32 Bytes (6 I/O, 26 Variable)	32 Bytes (6 I/O, 26 Variable)
Scratch Pad RAM	N/A	N/A	N/A	64 Bytes	64 Bytes	64 Bytes	64 Bytes	64 Bytes
EEPROM (Program) Size	256 Bytes, ~80 instructions	2K Bytes, ~500 instructions	2K Bytes, ~500 instructions	8 x 2K Bytes, ~4,000 inst.	8 x 2K Bytes, ~4,000 inst.	8 x 2K Bytes, ~4,000 inst.	8 x 2K Bytes, ~4,000 inst.	8 x 2K Bytes, ~4,000 inst.
Number of I/O pins	8	16 + 2 Dedicated Serial	16 + 2 Dedicated Serial	16 + 2 Dedicated Serial	16 + 2 Dedicated Serial	16 + 2 Dedicated Serial	16 + 2 Dedicated Serial	16 + 2 Dedicated Serial
Voltage Requirements	5 - 15 vdc	5 - 15 vdc	5 - 15 vdc	5 - 12 vdc	5 - 12 vdc	5 - 12 vdc	5 - 12 vdc	5 - 12 vdc
Current Draw @ 5V	1 mA Run / 25 µA Sleep	3 mA Run / 50 µA Sleep	3 mA Run / 50 µA Sleep	25 mA Run / 200 µA Sleep	25 mA Run / 200 µA Sleep	60 mA Run / 500 µA Sleep	60 mA Run / 500 µA Sleep	60 mA Run / 500 µA Sleep
Source / Sink Current per I/O	20 mA / 25 mA	20 mA / 25 mA	20 mA / 25 mA	30 mA / 30 mA	30 mA / 30 mA	30 mA / 30 mA	30 mA / 30 mA	30 mA / 30 mA
Source / Sink Current per unit	40 mA / 50 mA	40 mA / 50 mA per 8 I/O pins	40 mA / 50 mA per 8 I/O pins	60 mA / 60 mA per 8 I/O pins	60 mA / 60 mA per 8 I/O pins	60 mA / 60 mA per 8 I/O pins	60 mA / 60 mA per 8 I/O pins	60 mA / 60 mA per 8 I/O pins
PBASIC Commands***	32	42	42	45	45	45	45	45
PC Programming Interface	Serial (w/BS1 Serial Adapter)	Serial (9600 baud)	Serial (9600 baud)	Serial (9600 baud)	Serial (9600 baud)	Serial (9600 baud)	Serial (9600 baud)	Serial (9600 baud)
Windows Text Editor	Stampw.exe (v2.1 and up)	Stampw.exe (v1.04 and up)	Stampw.exe (v1.04 and up)	Stampw.exe (v1.06 and up)	Stampw.exe (v1.06 and up)	Stampw.exe (v1.091 and up)	Stampw.exe (v1.091 and up)	Stampw.exe (v1.091 and up)

Released Products	BS2p24-IC		BS2p40-IC		BS2pe-IC		BS2px-IC		Javelin Stamp	
	24-pin DIP	40-pin DIP	24-pin DIP	24-pin DIP	24-pin DIP	24-pin DIP	24-pin DIP	24-pin DIP	24-pin DIP	24-pin DIP
Package	1.2" x 0.6" x 0.4"	2.1" x 0.6" x 0.4"	1.2" x 0.6" x 0.4"	1.2" x 0.6" x 0.4"	1.2" x 0.6" x 0.4"	1.2" x 0.6" x 0.4"	1.2" x 0.6" x 0.4"	1.2" x 0.6" x 0.4"	1.24" x 0.60" x 0.45"	1.24" x 0.60" x 0.45"
Environment *	0° - 70° C (32° - 158° F)	0° - 70° C (32° - 158° F)	0° - 70° C (32° - 158° F)	0° - 70° C (32° - 158° F)	0° - 70° C (32° - 158° F)	0° - 70° C (32° - 158° F)	0° - 70° C (32° - 158° F)	0° - 70° C (32° - 158° F)	0° - 70° C (32° - 158° F)	0° - 70° C (32° - 158° F)
Microcontroller	Ubicom SX48AC	Ubicom SX48AC	Ubicom SX48AC	Ubicom SX48AC	Ubicom SX48AC	Ubicom SX48AC	Ubicom SX48AC	Ubicom SX48AC	Ubicom SX48AC	Ubicom SX48AC
Processor Speed	20 MHz Turbo	20 MHz Turbo	20 MHz Turbo	8 MHz Turbo	8 MHz Turbo	32 MHz Turbo	32 MHz Turbo	25 MHz Turbo	25 MHz Turbo	25 MHz Turbo
Program Execution Speed	~12,000 instructions/sec.	~12,000 instructions/sec.	~12,000 instructions/sec.	~6000/sec.	~6000/sec.	~19,000 instructions/sec.	~19,000 instructions/sec.	~8,500 instructions/sec.	~8,500 instructions/sec.	~8,500 instructions/sec.
RAM Size	38 Bytes (12 I/O, 26 Variable)	38 Bytes (12 I/O, 26 Variable)	38 Bytes (12 I/O, 26 Variable)	38 Bytes (12 I/O, 26 Variable)	38 Bytes (12 I/O, 26 Variable)	38 Bytes (12 I/O, 26 Variable)	38 Bytes (12 I/O, 26 Variable)	38 Bytes (12 I/O, 26 Variable)	38 Bytes (12 I/O, 26 Variable)	32768 Bytes
Scratch Pad RAM	128 Bytes	128 Bytes	128 Bytes	128 Bytes	128 Bytes	128 Bytes	128 Bytes	128 Bytes	128 Bytes	N/A
EEPROM (Program) Size	8 x 2K Bytes, ~4,000 inst.	8 x 2K Bytes, ~4,000 inst.	8 x 2K Bytes, ~4,000 inst.	16 x 2K Bytes (16 K for source)	16 x 2K Bytes (16 K for source)	8 x 2K Bytes, ~4,000 inst.	8 x 2K Bytes, ~4,000 inst.	8 x 2K Bytes, ~4,000 inst.	8 x 2K Bytes, ~4,000 inst.	32768 Bytes
Number of I/O pins	16 + 2 Dedicated Serial	32 + 2 Dedicated Serial	32 + 2 Dedicated Serial	16 + 2 Dedicated Serial	16 + 2 Dedicated Serial	16 + 2 Dedicated Serial	16 + 2 Dedicated Serial	16 + 2 Dedicated Serial	16 + 2 Dedicated Serial	16
Voltage Requirements	5 - 12 vdc	5 - 12 vdc	5 - 12 vdc	5 - 12 vdc	5 - 12 vdc	5 - 12 vdc	5 - 12 vdc	5 - 12 vdc	5 - 12 vdc	5 - 24 vdc
Current Draw @ 5V	40 mA Run / 350 µA Sleep	40 mA Run / 350 µA Sleep	40 mA Run / 350 µA Sleep	15 mA Run / 36 µA Sleep	15 mA Run / 36 µA Sleep	80 mA Run / 450 µA Sleep	80 mA Run / 450 µA Sleep	80 mA Run / No Sleep	80 mA Run / No Sleep	80 mA Run / No Sleep
Source / Sink Current per I/O	30 mA / 30 mA	30 mA / 30 mA	30 mA / 30 mA	30 mA / 30 mA	30 mA / 30 mA	30 mA / 30 mA	30 mA / 30 mA	30 mA / 30 mA	30 mA / 30 mA	30 mA / 30 mA
Source / Sink Current per unit	60 mA / 60 mA per 8 I/O pins	60 mA / 60 mA per 8 I/O pins	60 mA / 60 mA per 8 I/O pins	60 mA / 60 mA per 8 I/O pins	60 mA / 60 mA per 8 I/O pins	60 mA / 60 mA per 8 I/O pins	60 mA / 60 mA per 8 I/O pins	60 mA / 60 mA per 8 I/O pins	60 mA / 60 mA per 8 I/O pins	60 mA / 60 mA per 8 I/O pins
PBASIC Commands***	61	61	61	61	61	63	63	63	63	0 (Java)
PC Programming Interface	Serial (9600 baud)	Serial (9600 baud)	Serial (9600 baud)	Serial (9600 baud)	Serial (9600 baud)	Serial (19200 baud)	Serial (19200 baud)	Serial (28800 baud)	Serial (28800 baud)	Serial (28800 baud)
Windows Text Editor	Stampw.exe (v1.1 and up)	Stampw.exe (v1.1 and up)	Stampw.exe (v1.1 and up)	Stampw.exe (v1.33 and up)	Stampw.exe (v1.33 and up)	Stampw.exe (v2.2 and up)	Stampw.exe (v2.2 and up)	Stampw.exe (v2.2 and up)	Stampw.exe (v2.2 and up)	Javelin Stamp IDE

\* 70% Non-Condensing Humidity  
 \*\* Industrial Models Available, -40° - 85° C (-40° - 185° F). Contact Parallax Sales for information.  
 \*\*\* Using PBASIC 2.5 for BS2-type models.

## Appendix E

Technical data for Board of Education Development Board™

### Board Of Education® - USB (#28850)

The Board Of Education (BOE) is a versatile, low-cost development platform designed for those interested in learning and using any of Parallax's 24-pin BASIC Stamp® microcontroller modules (not included). Its compact size, convenient features, and low price make it an ideal tool for the student and educator. For educators, the BOE provides a clean, efficient platform for our Stamps in Class Parts and Text Kits, or your own BASIC Stamp-based curriculum. (Note: also available in a Serial version, #28150.)

#### Features

- Accepts all 24-pin BASIC Stamp modules
- BASIC Stamp I/O pins plus power connections brought adjacent to a 2" x 1 3/8" breadboard
- Three-position power switch allows BASIC Stamp programming without providing power to -3-pin servo headers—very handy for robotics
- Jumper for selecting servo supply voltage: regulated ( $V_{dd} = 5\text{ V}$ ) or unregulated supply ( $V_{in}$ )
- 2.1 mm center-positive plug and 9-volt battery power supply

- connections, mechanically interlocked to prevent dual connection
- USB Mini-B connector to built-in USB to Serial circuit for BASIC Stamp programming and serial communication during run-time
- On-board 5 V regulator delivers up to 1 amp of current for larger projects
- Female 2 x 10 header for optional AppMod devices
- Grounded 0.125 in (3.18 mm) corner mounting holes, at 3.7 x 2.75 in (9.5 x 7 cm) on centers

### **Key Specifications**

- Power supply requirements: 6-9 VDC
- Communication: USB A to Mini-B to PC Operating temp.: 32-158 °F (0-70 C)
- Dimensions: 3.05 x 4 in (7.75 x 10.16 cm)

### **Packing List**

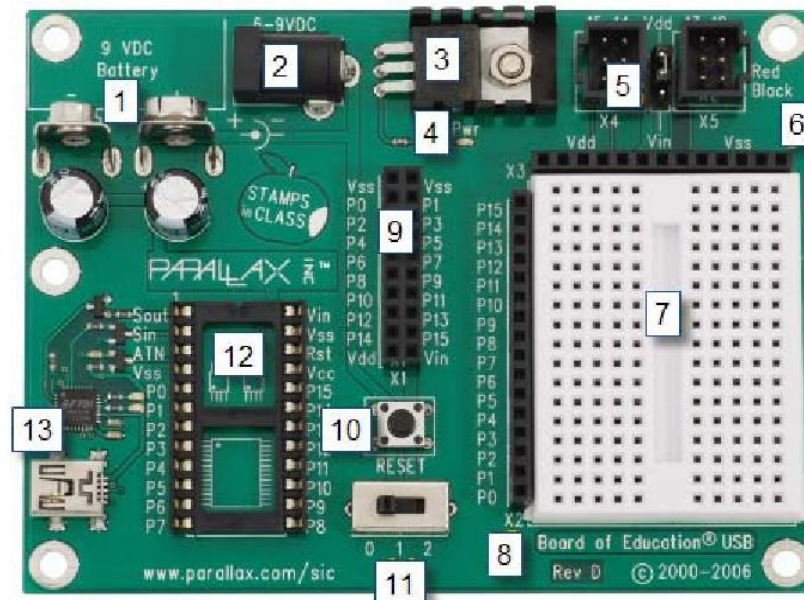
- Board of Education-USB PCB
- 3-inch Jumper Wires - 1 bag of 10
- 4 rubber feet

### **Additional Items Required**

- 24-pin BASIC Stamp module (see the Comparison Chart at [www.parallax.com/basicstamp.](http://www.parallax.com/basicstamp))
- USB A to Mini-B cable (#805-00006)

- 9 V battery — OR — a compatible 6-9 V power supply with a 2.1 mm center-positive plug. -We recommend our 7.5 V, 1 amp supply (#750-00009).
- PC running Windows 2K/XP/Vista/7 for the BASIC Stamp Editor software (a free download from [www.parallax.com/basicstampsoftware](http://www.parallax.com/basicstampsoftware)). USB drivers are included with the software installer.

### Board of Education - USB Features



1. **9V Battery Clip:** You can use alkaline or rechargeable 9 volt batteries. The battery clip and barrel jack are intentionally positioned so you cannot use both at once.

2. **Barrel Jack:** This accepts a 2.1 mm center-positive barrel plug from a 6-9 V wall-mount supply or from a battery pack. You cannot use the barrel jack and a 9 volt battery at the same time.
  
3. **Voltage regulator:** Supplies regulated 5 V (up to 1 amp of current) for sockets and pins labeled Vdd. Vdd sockets are convenient for supplying 5 V to circuits you will build on the breadboard area.
  
4. **Power Indicator LED:** This LED will light up when power is supplied to your board and the power switch is in position 1 or 2.
  
5. **Servo headers (X4 and X5) and Power Select Jumper:**

These each have two 3-pin connectors that bring power, ground, and I/O pin access together so you can easily plug in servos or other 3-pin devices. The power connection is pre-set to Vdd (+5 V) but you can set it to Vin (the board's supply voltage) by moving the shorting block on the jumper between the headers. Each 3-pin row is labeled with an I/O pin number above it. The 12, 13, 14, and 15 signal lines for the servo headers are also accessible as P12, P13, P14, and P15 I/O pin sockets on the X1 and X2 headers. This can be useful for building a servo signal indicator light on the breadboard as you may do in some Stamps in Class activities. For independent projects, keep these shared connections in mind, especially to avoid inadvertently connecting circuits with conflicting

functions to the same I/O pin.

6. **Power header (X3):** The sockets labeled Vdd connect to +5 VDC, Vin connects directly to the power supplied to the board by the battery clip or barrel jack, and Vss connects to 0 V (ground).
  
7. **Breadboard:** The breadboard has metal clips that run underneath the white plastic board in a horizontal fashion. Each strip connects a 5-socket group, with two groups to each row, separated by a center trench. Wires or legs of components plugged into the same 5-socket group will be electrically connected. Components with many legs (such as pushbuttons or ICs), are placed in the middle of the board so that half of the legs are on the left side and half are on the right side of the trench. Note: Always disconnect power before building or modifying circuits!
  
7. **I/O Pin Access Header (X2):** The BASIC Stamp module's 16 I/O pins, labeled 0 to 15, are connected to this header. Its location adjacent to the breadboard makes it convenient for connecting circuits to I/O pins. Keep in mind that I/O pin access is also brought to the X4, X5, and X1 headers, so be careful not to build conflicting breadboard circuits if you are using these other headers as well.
  
8. **AppMod header (X1):** The AppMod header provides power, I/O pins,

Vdd, Vin, and Vss access for any devices that are designed to use this 2x10 socket. Examples include the LCD Terminal AppMod (#29121), CMUcam (#30051), Easy Bluetooth Module (#30085), and Say It voice recognition module (#30080).

9. **Reset Button:** The reset button can be used to restart your BASIC Stamp without having to cycle the power. This saves wear-and-tear on the power switch for simple program restarts. Some advanced programming techniques use the reset button and the BASIC Stamp EEPROM program and data storage as a way to toggle between different program functions.
  
10. **3-Position Power Switch:** The leftmost position (0) is OFF - all power is disconnected. Always place the switch in this position when adding or changing components on the breadboard. The middle position (1) provides Vin (unregulated battery or power supply voltage) to the regulator, the BASIC Stamp socket, and to the connectors marked "Vin." This switch position also makes Vdd (5 volts) available to Vdd sockets on the breadboard and AppMod connectors. The rightmost position (2) also provides power to the servo connectors X4 and X5. Especially if your program causes a robot with servos connected to X4/X5 to start moving immediately, you can keep the 3- position switch in position (1) while loading the program, then switch to position (2) when you are ready for the robot to start moving.

11. **Socket for BASIC Stamp:** This socket is compatible with all 24-pin BASIC Stamp modules. It connects the BASIC Stamp to the programming connector, power, the power indicator LED, reset button, and all I/O pin headers.
13. **USB Programming Connector:** This is a USB Mini B socket and USB to serial (RS232) circuitry for programming and for two-way serial communication between the BASIC Stamp and your computer. The required USB drivers for Windows were included in the BASIC Stamp Editor Software installer; see the [www.parallax.com/basicstampsoftware](http://www.parallax.com/basicstampsoftware) page for more information.

## Appendix F

Technical data for Sensirion SHT 1X™ temperature and humidity probe

### Temperature

Parameter	Condition	min	typ	max	Units
Resolution <sup>1</sup>		0.04	0.01	0.01	°C
		12	14	14	bit
Accuracy <sup>2</sup> SHT10	typical		±0.5		°C
	maximal	see Figure 3			
Accuracy <sup>2</sup> SHT11	typical		±0.4		°C
	maximal	see Figure 3			
Accuracy <sup>2</sup> SHT15	typical		±0.3		°C
	maximal	see Figure 3			
Repeatability			±0.1		°C
Operating Range		-40		123.8	°C
		-40		254.9	°F
Response Time <sup>6</sup> $\tau$ (63%)		5		30	s
Long term drift			< 0.04		°C/yr

### Relative Humidity

Parameter	Condition	min	typ	max	Units
Resolution <sup>1</sup>		0.4	0.05	0.05	%RH
		8	12	12	bit
Accuracy <sup>2</sup> SHT10	typical		±4.5		%RH
	maximal	see Figure 2			
Accuracy <sup>2</sup> SHT11	typical		±3.0		%RH
	maximal	see Figure 2			
Accuracy <sup>2</sup> SHT15	typical		±2.0		%RH
	maximal	see Figure 2			
Repeatability			±0.1		%RH
Hysteresis			±1		%RH
Non-linearity	linearized		<<1		%RH
Response time <sup>3</sup> $\tau$ (63%)			8		s
Operating Range		0		100	%RH
Long term drift <sup>4</sup>	normal		< 0.5		%RH/yr